J. Fluid Mech. (2004), *vol.* 506, *pp.* 157–185. © 2004 Cambridge University Press
DOI: 10.1017/S0022112004008420 Printed in the United Kingdom

A slope-dependent disjoining pressure for non-zero contact angles

By QINGFANG WU AND HARRIS WONG†

Department of Mechanical Engineering, Louisiana State University, Baton Rouge, LA 70803-6413, USA

(Received 27 May 2003 and in revised form 11 December 2003)

A thin liquid film experiences additional intermolecular forces when the film thickness h is less than roughly 100 nm. The effect of these intermolecular forces at the continuum level is captured by the disjoining pressure Π. Since Π dominates at small film thicknesses, it determines the stability and wettability of thin films. To leading order, $\Pi = \Pi(h)$ because thin films are generally uniform. This form, however, cannot be applied to films that end at the substrate with non-zero contact angles. A recent *ad hoc* derivation including the slope h_x leads to $\Pi = \Pi(h, h_x)$, which allows non-zero contact angles, but it permits a contact line to move without slip. This work derives a new disjoining-pressure expression by minimizing the total energy of a drop on a solid substrate. The minimization yields an equilibrium equation that relates Π to an excess interaction energy $E = E(h, h_x)$. By considering a fluid wedge on a solid substrate, $E(h, h_x)$ is found by pairwise summation of van der Waals potentials. This gives in the small-slope limit

$$\Pi = \frac{B}{h^3}\left(\alpha^4 - h_x^4 + 2hh_x^2h_{xx}\right),$$

where α is the contact angle and B is a material constant. The term containing the curvature h_{xx} is new; it prevents a contact line from moving without slip. Equilibrium drop and meniscus profiles are calculated for both positive and negative disjoining pressure. The evolution of a film step is solved by a finite-difference method with the new disjoining pressure included; it is found that $h_{xx} = 0$ at the contact line is sufficient to specify the contact angle.

1. Introduction

A molecule in a bulk liquid is subject to intermolecular forces. A molecule in a thin liquid film may experience additional intermolecular forces if the film thickness is less than roughly 100 nm. The additional forces arise from the molecule's proximity to different materials or phases sandwiching the thin film. These forces can come from various sources, such as electrostatic or dipole–dipole interactions or a combination of the two (Israelachvili 1992). An uncharged and non-polar molecule has an instantaneous dipole that can induce polarization on others to create a net attraction between molecules. This gives rise to dispersion forces which usually are the main contribution to the van der Waals force (Mahanty & Ninham 1976; Israelachvili 1992). Thin-film forces can be studied by pressing a bubble in liquid against a solid surface. For some gas–liquid–solid systems a uniform thin film persists to separate the

† Author to whom correspondence should be addressed: hwong@lsu.edu.

https://doi.org/10.1017/S0022112004008420 Published online by Cambridge University Press

bubble from the solid. The film can sustain compression and its thickness decreases with increasing pressure. By varying the bubble pressure, this repulsive or disjoining pressure Π in the film can be measured as a function of film thickness h (Derjaguin *et al.* 1978). Similar measurements can be made on a freely suspended liquid film supported by a solid frame (Ivanov 1988). Nowadays, intermolecular forces between solid–solid surfaces are routinely studied by the atomic force microscope (Israelachvili 1992; Lee & Sigmund 2002). Owing to the historical development, thin-film forces per unit area are commonly referred to as disjoining pressure.

Disjoining pressure dominates at small film thicknesses and therefore governs the stability and wettability of thin films. For example, the exposed part of the eyeball is protected by a tear film, which is deposited by the rising meniscus of the upper lid during a blink (Wong, Fatt & Radke 1996). After deposition, a tear film thins rapidly near the lid meniscus and may break before the next blink if the disjoining pressure is destabilizing. Repeated rupture of the tear film may cause epithelium desiccation and corneal ulceration.

In the lung, airways are lined with a liquid film. Normal lungs produce surfactants to reduce the surface tension of the liquid film. Insufficient surfactants can lead to closure of small airways which can cause respiratory difficulties. An effective treatment for surfactant deficiency is to inhale surfactant-laden aerosols. As a surfactant droplet spreads on a liquid film, a shock forms followed by a thin region, which may break in a finite time if the disjoining pressure is destabilizing (Jensen & Grotberg 1992).

Thin-film forces also control the wettability of solid surfaces. A polymer film on a silicon wafer grafted with a bimodal polymer brush maintains a uniform thickness if the outside medium is air. However, when the polymer film is covered by water, it breaks into droplets, which re-spread to form a continuous film when water is removed (Reiter *et al.* 1999). Changing the outside medium from air to water alters the sign of the disjoining pressure, switching it from stabilizing to destabilizing.

Disjoining pressure may also be changed by irreversible adsorption. A water-wet surface covered by a water film has a stabilizing disjoining pressure. However, if the non-wetting phase is asphaltic oil with high-molecular-weight aggregates, and if the water film is pressed very thin, then the asphaltene aggregates may adsorb irreversibly onto the solid surface and change it into oil-wet. On an oil-wet surface, an oil film is stable whereas a water film is not. Thus, the disjoining pressure has been altered. This irreversible alteration can explain the geological development of mixed wettability in oil-reservoir rock (Kovscek, Wong & Radke 1993). A drainage model based on the irreversible alteration reproduces a range of phenomena associated with oil recovery from mixed-wet porous media.

Given the importance of disjoining pressure in controlling the stability and wettability of thin films, it is critical that an accurate model of disjoining pressure be developed. Since thin films are generally uniform, disjoining pressure can be taken to leading order as a function of film thickness only: $\Pi = \Pi(h)$. For van der Waals forces, this leads to $\Pi = A/6\pi h^3$, where A is the Hamaker constant (Israelachvili 1992). This expression has been applied to simulate equilibrium profiles (Deryagin, Starov & Churaev 1976; Renk, Wayner & Homsy 1978; Wong, Morris & Radke 1992*a*) and the evolution of non-uniform films (Oron, Davis & Bankoff 1997 and references therein). It has even been extended to model film breakup (Zhang & Lister 1999; Vaynblat, Lister & Witelski 2001) and spreading (Pismen, Rubinstein & Bazhlekov 2000; Davis & Troian 2003) in which film thickness $h \to 0$. Since this disjoining pressure becomes unbounded as $h \to 0$, its validity in modelling films that end at the substrate has been questioned.

https://doi.org/10.1017/S0022112004008420 Published online by Cambridge University Press

Hocking (1993) attempted to rectify this deficiency by deriving a disjoining pressure that depends not only on the film thickness, but also on the film slope. His derivation is based on the work of Miller & Ruckenstein (1974). They considered a liquid wedge on a solid substrate and calculated intermolecular potential Φ^* at a point on the liquid–vapour interface assuming van der Waals interactions between liquid–liquid and liquid–solid molecules and neglecting vapour contribution. They found that Φ^* is constant along the liquid–vapour interface at a particular wedge angle ψ. The liquid wedge is then taken to be at equilibrium with the contact angle ψ. Hocking (1993) took $\Pi = \Phi^*$, and allowed the slope of the wedge h_x to be different from the equilibrium value. In the small-slope limit, he obtained

$$\Pi = -\frac{B^*}{h^3}\left(\psi^4 - h_x^4\right), \tag{1.1}$$

where B^* and ψ depend on the van der Waals potentials and number densities. There are two problems with this derivation. First, Φ^* being constant at the interface does not imply equilibrium because Φ^* still varies inside the liquid wedge. (A proper equilibrium condition should be that Φ^* is constant everywhere.) Second, taking $\Pi = \Phi^*$ is unjustified. Recently, Indeikina & Chang (1999) also derived a disjoining pressure that depends on the slope. They likewise summed van der Waals potentials, but the liquid domain has a curved surface. Their derivation again lacks a rigorous equilibrium condition. As a result, the relation between intermolecular potential and disjoining pressure is similarly unjustified.

In this work, equilibrium conditions are derived by minimizing the total energy of a drop on a substrate that includes an excess energy E due to intermolecular interactions (§ 2). This potential energy E is assumed to depend on both film height h and film slope h_x. The minimization yields the augmented Young–Laplace equation, in which

$$\Pi = -\frac{\partial E}{\partial h} + \frac{\mathrm{d}}{\mathrm{d}x}\left(\frac{\partial E}{\partial h_x}\right), \tag{1.2}$$

where x is a coordinate along the solid surface. To find $E = E(h, h_x)$, we again consider a liquid wedge on a substrate and calculate the intermolecular potential Φ at a point in the liquid (§ 3). We argue that

$$E = \int_0^h (\Phi - \Phi_\infty)\,\mathrm{d}y, \tag{1.3}$$

where Φ_∞ is the bulk value of Φ far from the solid substrate, and y is a coordinate normal to the solid surface. This gives in the small-slope limit,

$$\Pi = -\frac{B}{h^3}\left(\alpha^4 - h_x^4 + 2hh_x^2h_{xx}\right), \tag{1.4}$$

where α is the contact angle and B is a material constant. This equation differs from Hocking's in that a higher-order term appears and the contact angle α is no longer the wedge angle.

When a liquid film ends at a substrate, an infinite-force singularity results at the contact line if the film is to be moved along the substrate (Dussan V. & Davis 1974). The singularity arises because a fluid particle has to turn through a finite angle at the contact line within an infinitesimal distance (Dussan V. 1979). Molecular-dynamics simulations have shown that liquid molecules slip on the solid surface to relieve the infinite force (Koplik, Banavar & Willemsen 1989; Thompson & Robbins 1989; Barrat & Bocquet 1999). Different slip models have been proposed (Oron *et al.* 1997;

https://doi.org/10.1017/S0022112004008420 Published online by Cambridge University Press

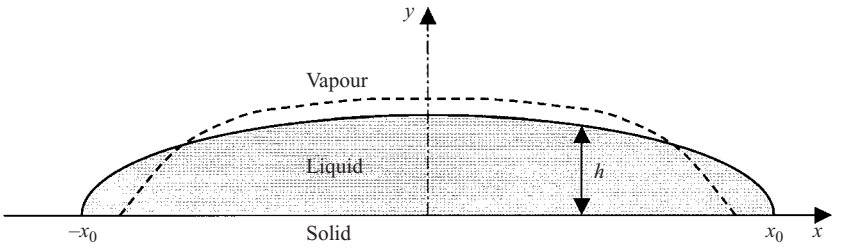


FIGURE 1. A two-dimensional drop on a solid substrate. The drop is in thermodynamic equilibrium and is symmetric about the y-axis. The drop width is $2x_0$ and the drop height is denoted by h. The dashed line represents a perturbed drop shape.

Shikhmurzaev 1997). Hocking's disjoining pressure allows a contact line to move without slip, in disagreement with the simulation results. Our disjoining pressure contains an extra higher-order term, which prevents a contact line from moving without slip.

The new disjoining pressure is used to solve equilibrium drop and meniscus shapes in § 4. We recover solutions for $\Pi = A/6\pi h^3$ when the liquid film does not end at the substrate. In addition, the slope-dependent disjoining pressure allows a new class of shapes including a planar wedge, a curved wedge and a drop. The evolution of a semi-infinite uniform film is simulated numerically in § 5. We show that the contact line cannot move without slip when the new disjoining pressure is included in the evolution equation. The model problem also illustrates the proper boundary conditions at the contact line. The linear stability of uniform films is studied in § 6. Further discussion is provided in § 7 and this work is concluded in § 8.

2. Minimization of the total energy

Consider a two-dimensional liquid drop on a smooth solid surface and in thermodynamic equilibrium with its own vapour, as illustrated in figure 1. This system has surface energies and an excess interaction energy E per unit substrate area due to thin-film forces. At equilibrium, the total energy of the system is at a minimum and its variation is zero:

$$\delta \int_0^{x_0} \left[\sigma\left(1 + h_x^2\right)^{1/2} + \sigma_{fs} - \sigma_{sg} + E + p_c h\right] \mathrm{d}x = 0, \tag{2.1}$$

where δ represents the variation of a function (Courant & Hilbert 1953), h is the film height, x is a horizontal coordinate with origin at the centre of the drop, $h_x = \mathrm{d}h/\mathrm{d}x$, σ is the liquid–vapour surface tension, σ_{fs} and σ_{sg} are the liquid–solid and solid–vapour surface tensions respectively, and x_0 is the half-width of the drop. Owing to symmetry, only half of the drop is considered. The first term in the integral represents the surface energy of the liquid–vapour interface. The second and third represent the net surface energy at the liquid–solid interface; if the liquid–solid interface lengthens, then the system gains liquid–solid surface energy but loses solid–vapour surface energy. Conservation of mass is imposed by a Lagrange multiplier p_c. The excess interaction energy E is a function of film thickness and film slope: $E = E(h, h_x)$. Equation (2.1) can be derived rigorously by use of thermodynamics (Yeh, Newman &

https://doi.org/10.1017/S0022112004008420 Published online by Cambridge University Press

Radke 1999). Expansion of (2.1) gives

$$\int_0^{x_0}\left(\frac{\partial E}{\partial h}+p_c\right)(\delta h)\,\mathrm{d}x+\int_0^{x_0}\left[\frac{\sigma h_x}{\left(1+h_x^2\right)^{1/2}}+\frac{\partial E}{\partial h_x}\right](\delta h_x)\,\mathrm{d}x + \left[\sigma\left(1+h_x^2\right)^{1/2}+\sigma_{fs}-\sigma_{sg}+E\right]_{x_0}\delta x_0=0, \quad (2.2)$$

where the drop-edge position is allowed to vary (by δx_0). Since $\delta h_x = \mathrm{d}(\delta h)/\mathrm{d}x$, the second integral is expanded via integration by parts:

$$\int_0^{x_0}\left[\frac{\partial E}{\partial h}+p_c-\frac{\sigma h_{xx}}{\left(1+h_x^2\right)^{3/2}}-\frac{\mathrm{d}}{\mathrm{d}x}\left(\frac{\partial E}{\partial h_x}\right)\right]\delta h\,\mathrm{d}x-\left[\frac{\sigma h_x}{\left(1+h_x^2\right)^{1/2}}+\frac{\partial E}{\partial h_x}\right]\delta h\Bigg|_{x=0} + \left[\frac{\sigma}{\left(1+h_x^2\right)^{1/2}}+\sigma_{fs}-\sigma_{sg}+E-h_x\frac{\partial E}{\partial h_x}\right]_{x=x_0}\delta x_0=0, \quad (2.3)$$

where $\delta h|_{x=x_0} = -h_x\,\delta x_0|_{x=x_0}$. Since δh is arbitrary, the above equation yields three conditions that govern the equilibrium shape of a drop on a solid surface.

The first coefficient leads to the augmented Young–Laplace equation in two dimensions:

$$\frac{\sigma h_{xx}}{\left(1+h_x^2\right)^{3/2}}-\frac{\partial E}{\partial h}+\frac{\mathrm{d}}{\mathrm{d}x}\left(\frac{\partial E}{\partial h_x}\right)=p_c. \quad (2.4)$$

By comparing with the usual augmented Young–Laplace equation (Wong *et al.* 1992*b*; Yeh *et al.* 1999), a disjoining pressure Π can be defined as

$$\Pi=-\frac{\partial E}{\partial h}+\frac{\mathrm{d}}{\mathrm{d}x}\left(\frac{\partial E}{\partial h_x}\right), \quad (2.5)$$

and the Lagrange multiplier p_c is recognized as the difference between vapour pressure p_g and liquid pressure p_f:

$$p_c=p_g-p_f. \quad (2.6)$$

The second and third terms in (2.3) serve as boundary conditions for the augmented Young–Laplace equation. At $x = 0$,

$$\frac{\sigma h_x}{\left(1+h_x^2\right)^{1/2}}+\frac{\partial E}{\partial h_x}=0. \quad (2.7)$$

At $x = x_0$,

$$\frac{\sigma}{\left(1+h_x^2\right)^{1/2}}+\sigma_{fs}-\sigma_{sg}+E-h_x\frac{\partial E}{\partial h_x}=0. \quad (2.8)$$

At this stage of the derivation, the slope h_x need not be small. The above equations reduce to that of Yeh *et al.* (1999) if $E = E(h)$ only. To complete the derivation, it remains to find an expression for the excess interaction energy E.

3. A disjoining pressure for non-zero contact angles

To derive an expression for $E = E(h, h_x)$, we consider a liquid wedge on a solid substrate as shown in figure 2. The liquid wedge is in equilibrium with its vapour. A liquid molecule M interacts with another molecule N in solid (s), liquid (f), or vapor (g) through the van der Waals potential,

$$\phi_{fs}=\frac{-\beta_{fs}}{MN^6}, \quad \phi_{ff}=\frac{-\beta_{ff}}{MN^6}, \quad \phi_{fg}=\frac{-\beta_{fg}}{MN^6}. \quad (3.1)$$

https://doi.org/10.1017/S0022112004008420 Published online by Cambridge University Press

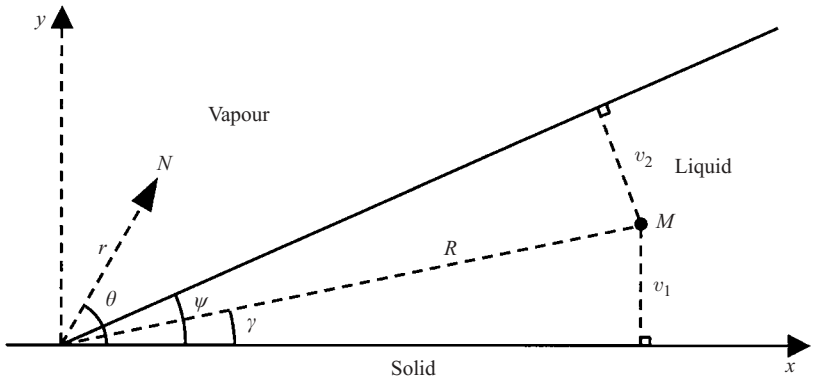


FIGURE 2. A liquid wedge on a solid substrate in equilibrium with its vapour. Cartesian coordinates (x, y, z) are defined at the tip of the wedge with z pointing out of the paper. An arbitrary point (or molecule) N in the domain can also be located by cylindrical coordinates (r, θ, z). A point (or molecule) M in the liquid has coordinates $(R, \gamma, 0)$ and is at a distance v_1 from the solid surface and v_2 from the wedge surface. The wedge angle is ψ.

The distance between M and N is denoted by MN, and β_{fs}, β_{ff}, and β_{fg} are the strengths of the van der Waals potentials. Following the usual practice, a cutoff distance is applied to the potential ϕ_{ff} to avoid infinite self-interactions. By summing the potential between M and other solid, liquid, and vapour molecules, we find the total intermolecular potential per unit volume at point M as (Appendix A)

$$\Phi = \frac{\pi n_f^2 \beta_{ff}}{6}\left[\frac{a_1(1-\rho)+\rho-\lambda}{v_1^3}+\frac{a_2(1-\rho)}{v_2^3}\right], \tag{3.2a}$$

$$\lambda = \frac{n_s\beta_{fs}}{n_f\beta_{ff}}, \quad \rho = \frac{n_g\beta_{fg}}{n_f\beta_{ff}}, \quad v_1 = R\sin\gamma, \quad v_2 = R\sin(\psi-\gamma), \tag{3.2b–e}$$

$$a_1 = \tfrac{1}{2}+\tfrac{3}{4}\cos\gamma-\tfrac{1}{4}\cos^3\gamma, \quad a_2 = \tfrac{1}{2}+\tfrac{3}{4}\cos(\psi-\gamma)-\tfrac{1}{4}\cos^3(\psi-\gamma), \tag{3.2f, g}$$

where n_s, n_f, and n_g are the number densities of the solid, liquid, and vapour molecules, v_1 is the height of point M from the solid surface, and v_2 is the distance between M and the wedge surface (figure 2). The wedge angle ψ will later yield the wedge slope h_x, and R and γ define the position of M (figure 2). The expression for Φ in (3.2a) holds for $\psi < 90°$. It can be reduced to the form used by Hocking (1993) when the vapour component is neglected ($\rho = 0$) and when M lies at the liquid–vapour interface.

The potential Φ is related to E in two steps. First, the bulk component Φ_∞ must be subtracted from Φ because Φ accounts for all intermolecular interactions including bulk and thin-film components, whereas E is an excess interaction energy due only to thin-film forces. The bulk component is the value of Φ far from the solid substrate, i.e. as v_1 tends to infinity but keeping v_2 fixed (figure 2):

$$\Phi_\infty = \frac{\pi n_f^2 \beta_{ff}(1-\rho)}{6v_2^3}. \tag{3.3}$$

In the second step, we note that $\Phi - \Phi_\infty$ is energy per unit volume and varies with (x, y), whereas E is energy per unit substrate area and depends only on x (figure 2).

https://doi.org/10.1017/S0022112004008420 Published online by Cambridge University Press

Thus, we take

$$E = \int_D^h (\Phi - \Phi_\infty)\,\mathrm{d}y. \tag{3.4}$$

A cut-off distance D has been imposed near the substrate to avoid infinite self-interactions (Appendix B). The integral is evaluated and in the limit $D/h \to 0$ becomes

$$E = -\frac{\pi n_f^2 \beta_{ff}}{4h^2}\left\{\frac{(1-\lambda)}{3} + \frac{(1-\rho)h_x^2}{4}\left[1 - \left(1+h_x^2\right)^{-1/2}\right]\right\}. \tag{3.5}$$

This expression holds for finite slopes. However, in the energy minimization, we have assumed $E = E(h, h_x)$ and have neglected the dependence on curvature. This is valid if $h_x \ll 1$, which implies $hh_{xx} \ll h_x$, i.e. the non-dimensionalized curvature is much smaller than the slope. Furthermore, most applications of disjoining pressure involve thin films, which are relatively flat. Thus, we take the limit $h_x \to 0$ and get

$$E = -\frac{\pi n_f^2 \beta_{ff}(1-\rho)}{32h^2}\left[\frac{8}{3}\left(\frac{1-\lambda}{1-\rho}\right) + h_x^4\right]. \tag{3.6}$$

This excess energy E holds for a liquid wedge with constant slope h_x. However, the liquid drop in figure 1 has variable slopes. Application of E to the drop is therefore an approximation that becomes increasingly accurate as the drop edge is approached. Since the edge is where thin-film forces are important, we deem this approximation acceptable.

Following the derivation in § 2, a disjoining pressure is found as

$$\Pi = -\frac{\partial E}{\partial h} + \frac{\mathrm{d}}{\mathrm{d}x}\left(\frac{\partial E}{\partial h_x}\right) = -\frac{B}{h^3}\left(\alpha^4 - h_x^4 + 2hh_x^2 h_{xx}\right), \tag{3.7a}$$

$$B = \frac{3\pi n_f^2 \beta_{ff}(1-\rho)}{16}, \quad \alpha = \left[\frac{8(1-\lambda)}{9(1-\rho)}\right]^{1/4}. \tag{3.7b, c}$$

If a liquid film is flat, $h_x = h_{xx} = 0$, and (3.7a) becomes

$$\Pi = -\frac{B\alpha^4}{h^3}, \tag{3.8}$$

which recovers the usual h^{-3} dependence of disjoining pressure. The negative sign indicates that Π in (3.8) is attractive. This follows from the long-range attractive intermolecular potential used in deriving E. However, disjoining pressure can be positive or negative (Israelachvili 1992). To explore all possible applications, we study both positive and negative disjoining pressure. Thus, (3.7a) is written

$$\Pi = \pm\frac{B}{h^3}\left(\alpha^4 - h_x^4 + 2hh_x^2 h_{xx}\right) \tag{3.9}$$

with $B > 0$ and the positive (negative) sign representing a positive (negative) disjoining pressure.

The new disjoining pressure allows a liquid film to end at a solid substrate with contact angle α. As the film height $h \to 0$, Π can remain bounded if $h_x \to \alpha$ and $hh_{xx} \to 0$ faster than or at the same rate as $h^3 \to 0$. As shown in the next section, this is realized if the interface is very flat near the contact line. Since the final expression for E assumes $h_x \ll 1$, the contact angle $\alpha \ll 1$.

The new disjoining pressure differs from Hocking's. Our expression contains a higher derivative h_{xx} that arises from assuming $E = E(h, h_x)$ instead of just $E = E(h)$.

https://doi.org/10.1017/S0022112004008420 Published online by Cambridge University Press

Thus, although we are aiming to include only the effect of the slope h_x, a curvature term appears and cannot be avoided. This curvature term plays a decisive role in preventing a contact line from moving without slip, as detailed in § 5.

4. Equilibrium film profiles

The augmented Young–Laplace equation in two dimensions follows from (2.4):

$$\sigma h_{xx} \pm \frac{B}{h^3}\left(\alpha^4 - h_x^4 + 2hh_x^2 h_{xx}\right) = p_c. \tag{4.1}$$

This equation holds for small slopes. The pressure difference $p_c = p_g - p_f$ between vapour pressure p_g and liquid pressure p_f can be positive or negative depending on the application. Equation (4.1) states that the capillary pressure σh_{xx} and the disjoining pressure must sum to a constant. Away from the contact line, the capillary pressure dominates. Near the contact line as $h \to 0$, (4.1) demands

$$|h_x| \to \alpha, \quad h_{xx} \to 0, \tag{4.2a, b}$$

for Π to be well-behaved. Thus, the capillary pressure vanishes at the contact line, and the pressure difference is balanced solely by the disjoining pressure.

Minimization of the total energy leaves two boundary conditions for the drop shape: one at the symmetry plane $x = 0$ and the other at the contact line $x = x_0$. Both (2.7) and (2.8) contain $\partial E/\partial h_x (= \pm 2Bh_x^3/3h^2)$. Equation (2.7) gives, at $x = 0$,

$$h_x = 0, \tag{4.3a}$$

which is simply the symmetry condition. As $x \to x_0$,

$$E - h_x \frac{\partial E}{\partial h_x} = \pm \frac{B\left(\alpha^4 - h_x^4\right)}{2h^2} \to 0, \tag{4.3b}$$

if (4.2a, b) hold and in addition, as $h \to 0$,

$$h_{xxx} \to 0. \tag{4.2c}$$

Consequently, (2.8) recovers the usual force balance in the horizontal direction at $x = x_0$:

$$\frac{\sigma}{\left(1 + h_x^2\right)^{1/2}} + \sigma_{fs} - \sigma_{sg} = 0. \tag{4.4}$$

This is Young's equation, which can determine the contact angle $\alpha = h_x(x_0) \ll 1$ if σ, σ_{fs}, and σ_{sg} are specified. Hence, α is assumed known for the rest of this paper.

The augmented Young–Laplace equation (4.1) is derived for a drop on a substrate. However, once derived, it may be applied to other situations. Here, we attempt to find all admissible solutions of (4.1). The equation can be made dimensionless by a film height h_0 (unspecified yet):

$$H = \frac{h}{h_0}, \quad X = \frac{\alpha x}{h_0}, \tag{4.5a, b}$$

$$H_{XX} \pm \varepsilon \left(\frac{1 - H_X^4 + 2HH_X^2 H_{XX}}{H^3}\right) = C, \tag{4.6}$$

$$\varepsilon = \frac{B\alpha^2}{\sigma h_0^2}, \tag{4.7}$$

$$C = \frac{p_c h_0}{\sigma \alpha^2}, \tag{4.8}$$

https://doi.org/10.1017/S0022112004008420 Published online by Cambridge University Press

where ε measures the ratio of disjoining to capillary pressure, which is small in most applications, and C is the non-dimensional pressure difference. This equation can be integrated once to give

$$H_X^2 = \frac{\pm 1}{2\varepsilon}(-H^2 + \sqrt{H^4 \pm 8\varepsilon C H^3 \pm 4K\varepsilon H^2 + 4\varepsilon^2}), \tag{4.9}$$

where K is an integration constant. Although the square root may also take a negative sign, only the positive sign yields physical solutions. If the liquid film ends at the substrate, (4.9) gives that, as $H \to 0$,

$$H_X^2 \to \pm 1. \tag{4.10}$$

Thus, only the positive disjoining pressure is admissible if a film ends at the substrate. Furthermore, as $H \to 0$, the only value of K in (4.9) that allows $(1 - H_X^4)/H^3$ in (4.6) to be bounded is

$$K = 1. \tag{4.11}$$

The dimensionless pressure difference C can be zero, negative, or positive depending on the application. These three cases are considered.

4.1. *Equilibrium profiles for* $C = 0$

If a liquid film ends at a substrate, then $K = 1$ in (4.9) and the disjoining pressure must be positive. Thus, (4.9) reduces to

$$H_X^2 = 1, \tag{4.12}$$

indicating that the film is a wedge with slope ± 1. This wedge solution holds for arbitrary ε. Since the derivation of Φ uses a wedge film, recovery of the wedge solution suggests self-consistency.

If a liquid film does not end at the substrate, then it must have at least one symmetry plane because (4.6) is invariant in changing X to $-X$. (The uniform-film solution is excluded by (4.6).) The film height h_0 at the symmetry plane provides a length scale: at $X = 0$, $H = 1$, and $H_X = 0$. This forces $K = -(\pm\varepsilon)$ in (4.9). However, K must be positive since in the limit $H \to \infty$, (4.9) gives

$$H_X^2 \to K. \tag{4.13}$$

Thus, only the negative disjoining pressure is acceptable and the symmetry condition yields

$$K = \varepsilon. \tag{4.14}$$

For $\varepsilon \ll 1$, the film is mildly inclined because $H_X \to \varepsilon^{1/2}$ as $H \to \infty$. The film profiles can be normalized by defining

$$\zeta = \varepsilon^{1/2} X. \tag{4.15}$$

Equation (4.13) gives that as $H \to \infty$,

$$H_\zeta \to 1. \tag{4.16}$$

Equation (4.6) with the negative disjoining pressure becomes

$$H_{\zeta\zeta} - \left(\frac{1 - \varepsilon^2 H_\zeta^4 + 2\varepsilon^2 H H_\zeta^2 H_{\zeta\zeta}}{H^3}\right) = 0. \tag{4.17}$$

https://doi.org/10.1017/S0022112004008420 Published online by Cambridge University Press

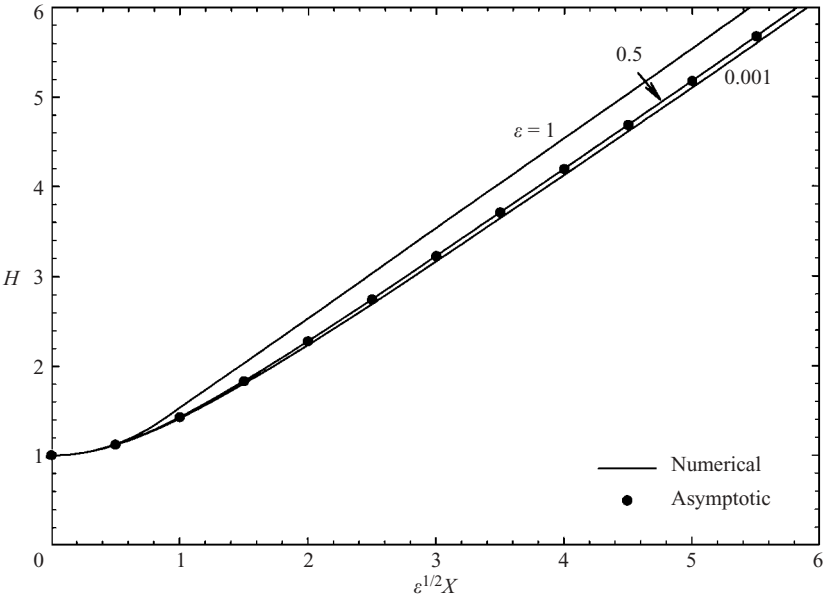


FIGURE 3. Symmetric valley film profiles for $C = 0$ and various ε. The asymptotic solution holds in the limit $\varepsilon \to 0$ and is listed in (4.18). The film height has been non-dimensionalized by the minimum height h_0, and $X = \alpha x/h_0$. Note that the horizontal axis is actually $\varepsilon^{1/2}X$ to normalize the film profiles.

This equation is solved numerically by a fourth-order Runge–Kutta method, and the computed profiles are plotted in figure 3 for various ε.

If $\varepsilon = 0$ in (4.17), the disjoining pressure reduces to the form that depends only on H. Hence, when the film does not end at the substrate, the slope-dependent terms have negligible $O(\varepsilon^2)$ contribution to Π. To discern their effects on the film profile, an asymptotic solution is sought in the limit $\varepsilon \to 0$ (Appendix C):

$$H(\zeta) = H_0(\zeta) + \varepsilon^2 H_1(\zeta) + \cdots, \tag{4.18a}$$

$$H_0 = (\zeta^2 + 1)^{1/2}, \tag{4.18b}$$

$$H_1 = \frac{\zeta}{4(\zeta^2+1)^{3/2}}[(\zeta^2+1)\tan^{-1}(\zeta) - \zeta]. \tag{4.18c}$$

As $\zeta \to 0$, $H_1 \to \zeta^4/6$. Thus, the slope-dependent terms have little effect on the minimum film profile. As $\zeta \to \infty$, $H_1 \to \pi/8 - 1/2\zeta$, so that the slope-dependent terms only increase the film height by a constant, but they have no effect on the far-field slope. This asymptotic solution is also plotted in figure 3. It agrees with the numerical results, even for $\varepsilon = 0.5$.

4.2. *Equilibrium profiles for* $C < 0$

If $C < 0$, the liquid pressure exceeds the vapour pressure, and two equilibrium solutions are found: a drop and a uniform film. For a drop, $K = 1$ and the disjoining pressure is positive because the drop surface contacts the substrate. At the drop centre, $h = h_0$ or $H = 1$ and symmetry demands $H_X = 0$. Thus, (4.9) gives

$$C = -\frac{1+\varepsilon}{2}. \tag{4.19}$$

https://doi.org/10.1017/S0022112004008420 Published online by Cambridge University Press

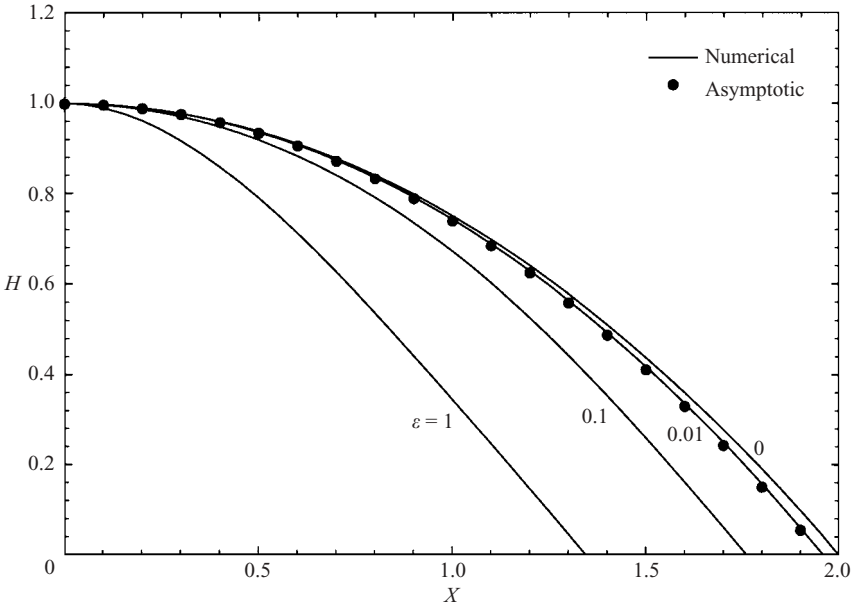


FIGURE 4. Equilibrium drop profiles for various ε. The dimensionless pressure jump is $C = -(1+\varepsilon)/2$. The profiles are non-dimensionalized such that the drop height is unity at the centre and the slope is unity at the edge. The asymptotic solution holds in the limit $\varepsilon \to 0$ and is listed in Appendix D.

Equation (4.6) is solved using a fourth-order Runge–Kutta method. The integration starts at $X = 0$ with $H = 1$ and $H_X = 0$; it stops when H becomes zero. Computed drop profiles are plotted in figure 4 for various ε. If $\varepsilon = 0$, the parabolic drop shape is recovered: $H = -X^2/4 + 1$. The contact line position is $X_0 = 2$ and the volume of half a drop is $V = 4/3$. As ε increases, the liquid drop becomes more pointed (figure 4) and both X_0 and V decrease (figure 5). The profiles in figure 4 are non-dimensionalized so that the drop height is unity at the centre and the slope is unity at the edge. In figure 5, the width is made dimensionless by h_0/α and the volume by h_0^2/α.

The limit $\varepsilon \to 0$ is singular and a boundary layer exists near the contact line. The singularity arises because disjoining pressure dominates as $H \to 0$ and its effect on the film profile is not uniform. The length scales in the inner region are found by balancing the dominant capillary-pressure and disjoining-pressure terms in (4.6): $\delta H \sim \delta X \sim \varepsilon^{1/2}$. Consequently, the drop profile is expanded in an asymptotic series of $\varepsilon^{1/2}$:

$$H = H_0 + \varepsilon^{1/2} H_1 + (\varepsilon \ln \varepsilon) H_2 + \varepsilon H_3 + \cdots, \tag{4.20a}$$

$$C = C_0 + \varepsilon^{1/2} C_1 + (\varepsilon \ln \varepsilon) C_2 + \varepsilon C_3 + \cdots, \tag{4.20b}$$

$$X_0 = X_{00} + \varepsilon^{1/2} X_{01} + (\varepsilon \ln \varepsilon) X_{02} + \varepsilon X_{03} + \cdots. \tag{4.20c}$$

The $\varepsilon \ln \varepsilon$ scale is suggested by the inner solution. In the inner region, we define

$$\eta = \frac{H}{\varepsilon^{1/2}}, \quad \xi = \frac{X - X_0}{\varepsilon^{1/2}}. \tag{4.21a, b}$$

The inner film height is similarly expanded:

$$\eta = \eta_0 + \varepsilon^{1/2} \eta_1 + \varepsilon \eta_2 + \cdots. \tag{4.22}$$

https://doi.org/10.1017/S0022112004008420 Published online by Cambridge University Press

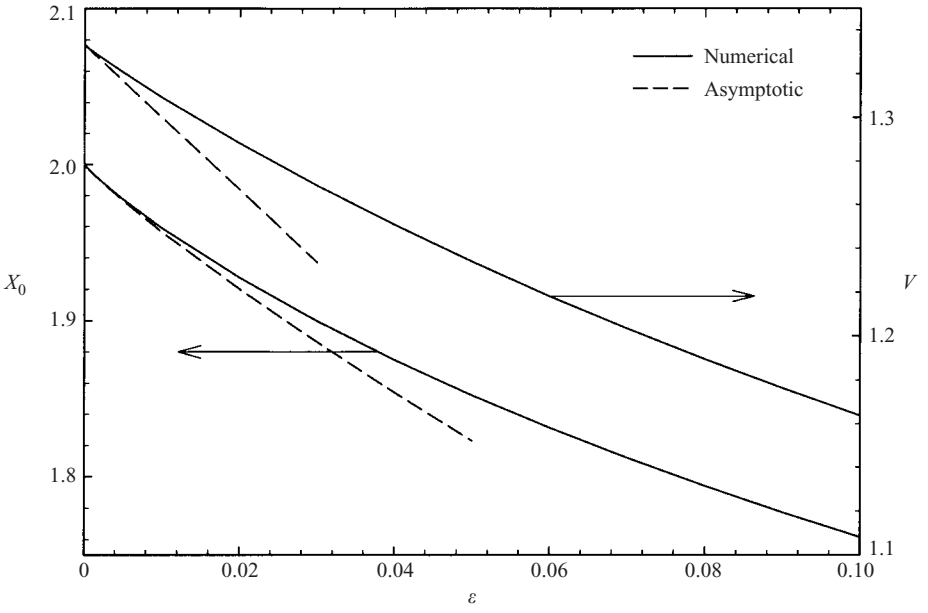


FIGURE 5. Half-width X_0 and half-volume V versus ε for the drops in figure 4. The width is made dimensionless by h_0/α and the volume by h_0^2/α. The asymptotic solutions hold in the limit $\varepsilon \to 0$ and are listed in (4.24) and (4.27).

Substitution into the governing equation, solving the outer and inner expansions, and matching yields (Appendix D)

$$C = -\tfrac{1}{2}(1+\varepsilon), \tag{4.23}$$

$$X_0 = 2 + \tfrac{1}{2}(\varepsilon \ln \varepsilon) - \left(1 + \tfrac{3}{2}\ln 2\right)\varepsilon, \tag{4.24}$$

$$H_1 = H_2 = 0, \tag{4.25}$$

and a composite solution for the film profile:

$$H_C = H + \varepsilon^{1/2}\eta - \lim_{\xi \to -\infty} \varepsilon^{1/2}\eta. \tag{4.26}$$

The half-drop volume is calculated as

$$V = \int_0^{X_0} H_c \mathrm{d}X = \tfrac{4}{3} - \tfrac{10}{3}\varepsilon. \tag{4.27}$$

The asymptotic expansion of C recovers the exact solution in (4.19). The composite film profile is plotted in figure 4 for $\varepsilon = 0.01$ and compares well with the numerical results. The asymptotic expansions of X_0 and V are graphed in figure 5 and agree with the computed values as $\varepsilon \to 0$. These comparisons validate both the numerical and asymptotic solutions.

Equation (4.6) also admits a uniform-film solution with $H = 1$ (i.e. $h = h_0$), $H_X = 0$, and $H_{XX} = 0$. Thus, (4.6) shows that the disjoining pressure must be negative, and

$$C = -\varepsilon. \tag{4.28}$$

The conjoining pressure pulls the film together to balance the pressure difference across the film surface. The dimensional film thickness $h_0 = (-B\alpha^4/p_c)^{1/3}$ follows from (4.28).

https://doi.org/10.1017/S0022112004008420 Published online by Cambridge University Press

4.3. *Equilibrium profiles for* $C > 0$

If $C > 0$, the vapour pressure is higher than the liquid pressure, and three equilibrium solutions are found: a uniform film, a uniform film that grows to a constant-curvature surface (figure 6), and a film wedge that grows to a constant-curvature surface (figure 7).

A uniform film has its thickness as a natural length scale: $H = 1$, $H_X = 0$, $H_{XX} = 0$. Thus (4.6) gives

$$C = \varepsilon. \tag{4.29}$$

Since $C > 0$, only the positive disjoining pressure is acceptable. The above equation yields the dimensional film thickness $h_0 = (B\alpha^4/p_c)^{1/3}$.

A uniform film can grow in the X-direction to approach a constant-curvature surface. The uniform thickness is perturbed as

$$H(X) = 1 + \delta(X). \tag{4.30}$$

Substitution into (4.6) and keeping only the linear terms of δ yields

$$\delta_{XX} - 3\varepsilon\delta = 0. \tag{4.31}$$

Only the positive disjoining pressure is acceptable, as demanded by the uniform film. Equation (4.31) admits two solutions: one growing and one decaying exponentially in X. The growing solution is of interest here:

$$\delta = a_m \exp\left(\sqrt{3\varepsilon}X\right). \tag{4.32}$$

The amplitude a_m needs to be small but its value has no physical significance; different values of a_m yield the same profile except for a shift in the origin of X. As a film grows, $H \gg 1$, and (4.9) shows $H_X^2 \to 2CH$ or

$$H_{XX} \to C. \tag{4.33}$$

Hence, the curvature becomes constant away from the wall. Since $C = \varepsilon$ for a uniform film, the curvature is small for $\varepsilon \ll 1$. Equations (4.31) and (4.32) suggest $X \sim \varepsilon^{-1/2}$ as $\varepsilon \to 0$. Thus, the film profiles are normalized in terms of the variable $\zeta = \varepsilon^{1/2}X$, and (4.6) becomes

$$H_{\zeta\zeta} + \left(\frac{1 - \varepsilon^2 H_\zeta^4 + 2\varepsilon^2 H H_\zeta^2 H_{\zeta\zeta}}{H^3}\right) = 1. \tag{4.34}$$

This equation is solved by a fourth-order Runge–Kutta method. At $\zeta = 0$, (4.32) provides the starting conditions: $H = 1 + \delta$ and $H_\zeta = \delta_\zeta$ with $a_m = 0.001$. Integrated film profiles are plotted as a function of ζ in figure 6 for various ε. They are insensitive to ε, because the slope-dependent terms in (4.34) are of order ε^2.

If $\varepsilon = 0$, (4.34) reduces to

$$H_{\zeta\zeta} + \frac{1}{H^3} = 1. \tag{4.35}$$

This equation has been studied by Deryagin *et al.* (1976) and Renk *et al.* (1978). By imposing the condition $H_\zeta = 0$ at $H = 1$, they found

$$\sqrt{2H+1} + \frac{1}{\sqrt{3}} \ln\left(\frac{\sqrt{2H+1} - \sqrt{3}}{\sqrt{2H+1} + \sqrt{3}}\right) = \zeta + K_1, \tag{4.36}$$

https://doi.org/10.1017/S0022112004008420 Published online by Cambridge University Press

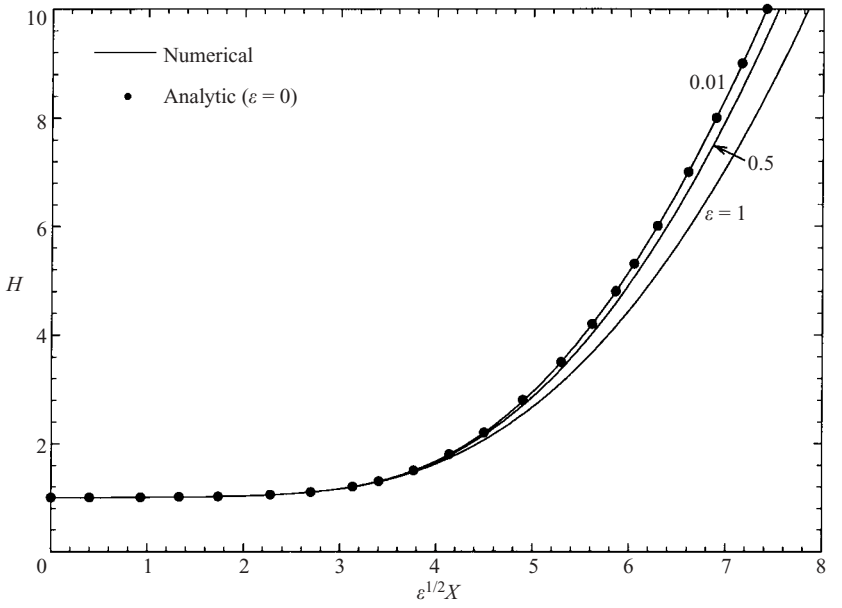


FIGURE 6. A uniform film growing to a parabolic film for various ε. The uniform section demands $C = \varepsilon$. Note the normalized horizontal axis. The analytic solution holds for $\varepsilon = 0$ and is listed in (4.36).

where K_1 is an integration constant and is determined by the film height at $\zeta = 0$. This solution is also plotted in figure 6 and compares well with the numerically integrated profile for $\varepsilon = 0.01$.

A film in contact with the substrate can also grow to approach a constant-curvature surface. At the contact line $X = 0$, the film grows initially with unit slope until $H_{XX} \to C$ as $H \to \infty$. Since there is no imposed length scale, we can take $C = 1$ (or $h_0 = \sigma\alpha^2/p_c$). Thus, ε is the only remaining parameter and (4.6) with the positive disjoining pressure becomes

$$H_{XX} + \varepsilon\left(\frac{1 - H_X^4 + 2HH_X^2H_{XX}}{H^3}\right) = 1. \tag{4.37}$$

Near the contact line as $X \to 0$, the above equation together with (4.2*a–c*) specifies

$$H \to X + \frac{X^4}{8\varepsilon} + \cdots. \tag{4.38}$$

This is used to start the integration of (4.37) at $X = 0.01$. Film profiles calculated by a fourth-order Runge–Kutta method are shown in figure 7 for various ε.

An asymptotic solution is obtained in the limit $\varepsilon \to 0$ to compare with the integrated film profiles. The film height is expanded in a series of $\varepsilon^{1/2}$ (Appendix E):

$$H = H_0 + \varepsilon^{1/2}H_1 + (\varepsilon \ln \varepsilon)H_2 + \varepsilon H_3 + \cdots. \tag{4.39}$$

The $\varepsilon \ln \varepsilon$ scale is needed for matching to the inner solution. In the inner region near the contact line, a set of variables is defined and expanded:

$$\eta = \frac{H}{\varepsilon^{1/2}}, \quad \xi = \frac{X}{\varepsilon^{1/2}}, \tag{4.40a, b}$$

$$\eta = \eta_0 + \varepsilon^{1/2}\eta_1 + \varepsilon\eta_2 + \cdots. \tag{4.41}$$

https://doi.org/10.1017/S0022112004008420 Published online by Cambridge University Press

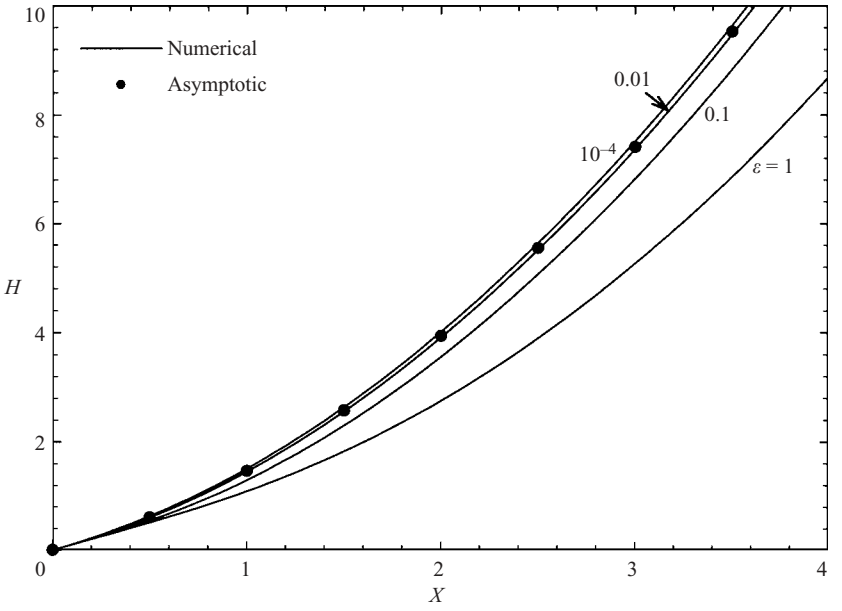


FIGURE 7. A wedge film growing to a parabolic film with curvature $C = 1$. The asymptotic solution holds in the limit $\varepsilon \to 0$ and the data are calculated using (4.42) for $\varepsilon = 0.01$.

The inner and outer asymptotic expansions are solved and matched to yield a composite solution for the film profile (Appendix E):

$$H_C = H + \varepsilon^{1/2}\eta - \lim_{\xi\to\infty} \varepsilon^{1/2}\eta. \tag{4.42}$$

This is plotted in figure 7 for $\varepsilon = 0.01$. It agrees with the numerically integrated profile.

5. Evolution of a film step

The new disjoining pressure prevents a contact line from moving without slip. This is demonstrated by a semi-infinite liquid film on a solid surface. Since the film is thin, gravity is taken as negligible. The augmented Young–Laplace equation in (4.1) gives the liquid pressure as

$$p_f = p_g - \sigma h_{xx} - \frac{\pm B}{h^3}\left(\alpha^4 - h_x^4 + 2hh_x^2 h_{xx}\right). \tag{5.1}$$

The film height $h = h(t, x)$ obeys (Oron *et al.* 1997)

$$\frac{\partial h}{\partial t} - \frac{1}{3\mu}\frac{\partial}{\partial x}\left(h^3\frac{\partial p_f}{\partial x}\right) = 0, \tag{5.2}$$

where t is time and μ is liquid viscosity. This equation holds for $h_x \ll 1$. A set of dimensionless variables can be defined based on the height h_0 of the uniform film:

$$H = \frac{h}{h_0}, \quad X = \frac{\alpha x}{h_0}, \quad \tau = \frac{t\sigma\alpha^4}{\mu h_0}, \tag{5.3a–c}$$

$$\frac{\partial H}{\partial \tau} + \frac{1}{3}\frac{\partial}{\partial X}\left\{H^3\frac{\partial}{\partial X}\left[H_{XX} \pm \frac{\varepsilon}{H^3}\left(1 - H_X^4 + 2HH_X^2 H_{XX}\right)\right]\right\} = 0, \tag{5.4}$$

where $\varepsilon = B\alpha^2/\sigma h_0^2$. Only the positive disjoining pressure is considered since the film surface contacts the substrate. Initially, at $\tau = 0$, the film consists of a wedge near

https://doi.org/10.1017/S0022112004008420 Published online by Cambridge University Press

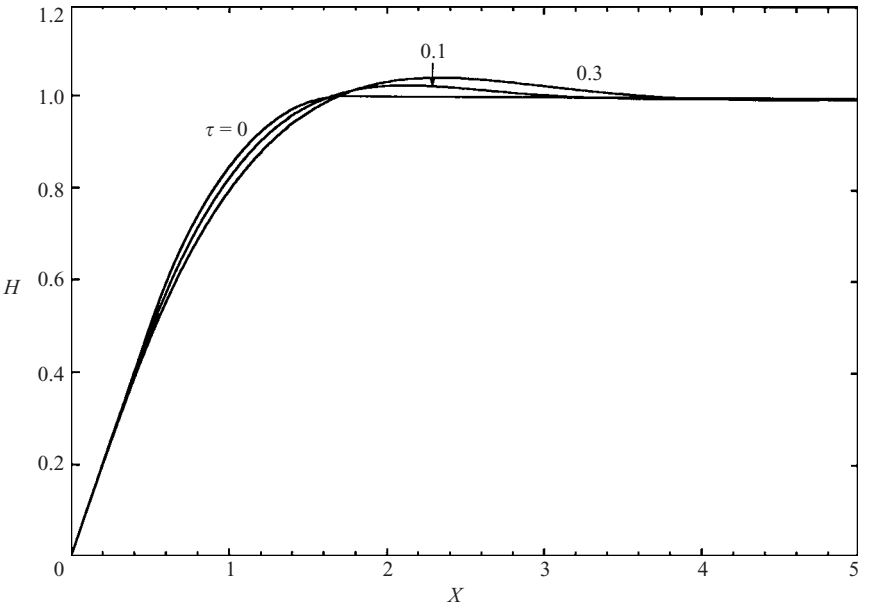


FIGURE 8. Evolving profiles of a thin film with fixed contact line at different times for $\varepsilon = 0.1$.

the contact line connected smoothly to a uniform film by a circular arc (figure 8). For $\tau > 0$, the film profile at the contact line must obey three boundary conditions: as $X \to 0$, $H \to 0$, $H_X \to 1$, and $H_{XX} \to 0$. These conditions are imposed by (5.4) for a well-behaved solution near the contact line. Thus, as $H \to 0$, (5.4) gives

$$H_\tau \to 8\varepsilon H_X^2 H_{XX}^2. \tag{5.5}$$

Thus, $H_\tau \to 0$ as $H \to 0$ and the contact line cannot move, because H_τ at the contact line is also the contact-line velocity for a film edge of unity slope. This differs from Hocking's results (see Discussion, § 7). Equation (5.4) is solved numerically by the Crank–Nicolson method with spatial derivatives replaced by second-order central differences. At each time step, the spatial derivatives are grouped in a descending order. In each group, only the highest-order derivative is evaluated at the current time; all other derivatives are found using the film height at the previous time step. This way of treating the nonlinearity yields a robust scheme. Boundary conditions at the fixed contact line $X = 0$ are $H = 0$ and $H_{XX} = 0$. Although the slope is not specified, the evolution equation forces $H_X \approx 1$ near the contact line. At the other end of the computational domain ($X = X_\infty$), the film is uniform: $H_X = 0$ and $H_{XXX} = 0$. Film profiles calculated with $X_\infty = 10$, $\Delta X = 0.01$, and $\Delta\tau = 0.001$ are plotted in figure 8 for $\varepsilon = 0.1$. By varying X_∞, ΔX, and $\Delta\tau$, the results are found to be accurate to four significant figures.

6. Stability of uniform films

A uniform film with normalized height $H = 1$ satisfies (5.4). Its stability is studied by adding a small perturbation:

$$H(\tau, X) = 1 + \delta(\tau, X). \tag{6.1}$$

https://doi.org/10.1017/S0022112004008420 Published online by Cambridge University Press

Since $|\delta| \ll 1$, (5.4) can be expanded in δ. The leading-order equation is linear in δ and amenable to a normal-mode analysis:

$$\delta(\tau, X) = \mathrm{e}^{\omega\tau} f(X), \tag{6.2}$$

$$\frac{\mathrm{d}^4 f}{\mathrm{d}X^4} - (\pm 3\varepsilon)\frac{\mathrm{d}^2 f}{\mathrm{d}X^2} + 3\omega f = 0. \tag{6.3}$$

The uniform-film solution holds for both positive and negative disjoining pressure. The eigenfunction is sinusoidal with wavenumber k:

$$f = \mathrm{e}^{\mathrm{i}kX}, \tag{6.4}$$

$$\omega = -\tfrac{1}{3}k^2(k^2 \pm 3\varepsilon). \tag{6.5}$$

Thus, the uniform film is stable if the disjoining pressure is positive. If the disjoining pressure is negative, the uniform film is stable if $k \geqslant (3\varepsilon)^{1/2}$, and unstable otherwise. These results are the same as those for $\Pi = \pm A/6\pi h^3$ (Ruckenstein & Jain 1974) because the slope and curvature terms in the new disjoining pressure are nonlinear in δ and they do not appear in (6.3).

The instability can be understood by a physical argument. If the film surface is perturbed by a sinusoidal wave, and if the disjoining pressure is negative, then the wave valleys would be closer to the substrate and would experience larger attractive forces. This would pull the valleys lower. Thus, the uniform film is unstable. This argument also applies to non-uniform films and suggests that the other equilibrium film profile in § 4 with the negative disjoining pressure is unstable.

7. Discussion

If $\Pi = A/6\pi h^3$, a liquid film on a solid substrate is not permitted to end at the substrate. A thin adsorbed film must cover the solid surface, but a meniscus can exist by attaching smoothly to the adsorbed film (Deryagin *et al.* 1976; Renk *et al.* 1978; Wong *et al.* 1992*a*). The new disjoining pressure $\Pi = \Pi(h, h_x, h_{xx})$ does allow direct contact between the film surface and the substrate, and Young's equation is satisfied at the contact line (§ 4). The new disjoining pressure admits a whole class of contact film profiles (§ 4). In addition, it also recovers the static solutions with an adsorbed film. For those solutions, the terms containing h_x and h_{xx} have a negligible $O(\varepsilon^2)$ effect on the film profile (§ 4). Thus, the new disjoining pressure is not a replacement but an extension of the previous expression.

Young's equation is obeyed at the contact line in the presence of disjoining pressure. This is the first time that Young's relation has been derived together with disjoining pressure. (Merchant & Keller (1992) verified Young's equation by summing intermolecular potentials, but they did not consider disjoining pressure.) In the work of Yeh *et al.* (1999), $E = E(h)$ only and Young's equation is not recovered because the extra term (E) in (2.8) is singular as $h \to 0$ and cannot be removed. This is acceptable in their formulation since the liquid film is not allowed to end at the substrate due to the singularity in $E(h)$ and there is no contact line. Hocking's (1993) and Indeikina & Chang's (1999) derivations of Π lack a rigorous equilibrium condition, and therefore (2.8) does not appear in their papers. In this work, equilibrium conditions arise naturally from energy minimization, resulting in (2.8) with two terms depending on E and $\partial E/\partial h_x$. When the expression for E obtained by summing intermolecular potentials is substituted into (2.8), the two terms can cancel each other

https://doi.org/10.1017/S0022112004008420 Published online by Cambridge University Press

and Young's equation (4.4) is recovered. This suggests that the current derivation of Π is self-consistent.

Surface tension results from molecular interactions, as does disjoining pressure. There is a question of how to separate the two effects. It has been suggested that surface tension is not constant in the region where disjoining pressure dominates. However, a non-uniform surface tension generates a Marangoni stress along the surface (Levich 1962; Wong, Rumschitzki & Maldarelli 1999). In the absence of surfactants, a Marangoni stress cannot be balanced and will always lead to fluid motion. Thus, surface tension should remain constant near a static contact line. The newly derived disjoining pressure does contain a curvature term: $2\varepsilon H^{-2}H_X^2H_{XX}$. This term may be viewed as a form of excess capillary pressure introduced by the disjoining pressure. This excess capillary pressure contains H^{-2} but is actually bounded as $H\to 0$ because the curvature $H_{XX}\to 0$ and $H_{XXX}\to 0$: $2\varepsilon H_X^2H_{XX}/H^2\to \varepsilon H_{XXXX}=3C$, as determined by (4.6). For a drop, $(C-\varepsilon)$ is the capillary pressure at the drop centre. Thus, the excess capillary pressure is significant near the contact line. The new disjoining pressure shows how the capillary pressure is modified without altering the value of surface tension.

The new disjoining pressure consists of two terms: $(1-H_X^4)/H^3$ and $2H_X^2H_{XX}/H^2$. Hocking's derivation has the first term, but not the second. The second term is responsible for preventing a contact line from moving without slip. The evolution equation (5.4) reduces to (5.5) at the contact line. Since $H_X\to 1$ and $H_{XX}\to 0$ as $H\to 0$, $H_\tau\to 0$ and the contact line cannot move. If the second term in the disjoining pressure is dropped in (5.4), then as $H\to 0$,

$$H_\tau \to \frac{14\varepsilon}{3}H_{XXX}. \tag{7.1}$$

Hence, if $H_{XXX}\neq 0$, then $H_\tau\neq 0$ and the contact line moves without slip. This is responsible for Hocking's regular solution of an inclined plate sliding into a pool of liquid. He found a steady solution of the interfacial profile even without slip, but not if the disjoining pressure is turned off. His conclusion disagrees with observations from molecular dynamics simulations. Our rigorous derivation yields the second term in the disjoining pressure, which describes correctly the behaviour of contact lines.

In § 3, the total intermolecular potential Φ between a liquid molecule and other solid, liquid, and vapour molecules is found. The molecules interact through van der Waals potentials with different strengths reflecting different materials. In addition, the final expression contains the number densities of the three phases. Thus, it is possible, for example, to replace the vapour with another liquid by substituting the appropriate van der Waals potential and number density. Hence, the new disjoining pressure applies not only to solid–liquid–vapour systems, but also to other combinations of phases.

The new disjoining pressure is derived assuming that molecules interact by van der Waals forces. Although van der Waals forces are one of the most common types of intermolecular force, their usage does have limitations. For example, only the negative disjoining pressure will induce instability in a uniform film (§ 6), but all equilibrium solutions of contacting films require positive disjoining pressure (§ 4). By the physical argument in § 6, negative disjoining pressure always lead to instability in equilibrium film profiles, and a liquid film must break in a finite time. However, after rupture, a film with negative disjoining pressure cannot approach an equilibrium shape, at least not in a form considered in this paper. It is unclear what geometry the film will finally assume. This difficulty arises from using van der Waals forces and may be eliminated if other intermolecular forces are incorporated. The energy minimization approach

https://doi.org/10.1017/S0022112004008420 Published online by Cambridge University Press

introduced in this work is sufficiently general that it can be applied to other forms of intermolecular interactions. Indeed, this is one of the main purposes of this work, i.e. to provide a rigorous framework for deriving disjoining-pressure isotherms.

8. Conclusions

We have derived rigorously a new form of disjoining pressure that depends on the slope as well as the curvature of the film surface. The derivation starts by minimizing the energy of a drop on a solid substrate. It leads to three equilibrium conditions: the augmented Young–Laplace equation governing the drop profile and two boundary conditions. The governing equation relates Π to an excess interaction energy $E(h, h_x)$. By considering a liquid wedge on a solid substrate, the intermolecular potential Φ between a liquid molecule and other molecules is found by pairwise summation of van der Waals potentials. The excess energy E follows by integrating Φ. This gives a new disjoining pressure. The boundary condition at the contact line reduces to Young's equation. This is the first time that Young's equation has been derived in the presence of disjoining pressure. Its recovery suggests that the derivation procedure is valid. The new disjoining pressure does not allow movement of a contact line if slip is not included. This agrees with results from molecular dynamics simulations. All acceptable equilibrium film profiles have been calculated from the augmented Young–Laplace equation. The negative disjoining pressure (attractive pressure) allows two solutions: a uniform film and a symmetric valley that extends to two planes. For positive disjoining pressure, acceptable solutions include a drop, a uniform film, a uniform film growing to a constant-curvature surface, a wedge film, and a wedge film growing to a constant-curvature surface. A uniform film with negative disjoining pressure is unstable to long-wave disturbances. For positive disjoining pressure, a uniform film is found to be linearly stable. The evolution of a film step has been solved numerically by a finite-difference method. It shows that the zero-curvature condition at the contact line is sufficient to maintain the contact angle.

We thank Peter Wayner, Joel Plawsky, and Clayton Radke for initiating our interest in this work, and Jin Zhang for providing the results in figure 8. The derivation procedure was first presented at the APS/DFD meeting in 2002 and at the ACS National meeting in 2003, and comments from the audience were helpful. We also benefited from referees' questions and suggestions. This work was supported by NASA (NAG3-2361 to H. W.) and NASA EPSCoR DGAP subprogram (NASA (1999-00)-DGAP-02 to H. W.).

Appendix A. The total intermolecular potential Φ per unit volume

Consider a liquid wedge on a solid substrate as shown in figure 2. At a point in the liquid wedge, the total intermolecular potential per unit volume is

$$\Phi = n_f(\Phi_{ff} + \Phi_{fs} + \Phi_{fg}), \tag{A 1}$$

where $n_f$is the number density of liquid, Φ_{ff} is the intermolecular potential between a liquid molecule M and the rest of the liquid wedge outside a sphere of radius D surrounding M, Φ_{fs} is the intermolecular potential between M and the semi-infinite solid substrate, and Φ_{fg} is that between M and the vapour. A cylindrical coordinate system (r, θ, z) is defined for a point N, with z perpendicular to x and y (figure 2). In terms of these coordinates, the liquid molecule M is located at $(R, \gamma, 0)$. Thus, the

https://doi.org/10.1017/S0022112004008420 Published online by Cambridge University Press

distance MN between M and N can be found from

$$MN^2 = R^2 + r^2 + z^2 - 2rR\cos(\theta - \gamma). \tag{A 2}$$

This gives

$$\Phi_{fs} = \iiint_{V_s} n_s \phi_{fs}\, \mathrm{d}V = \int_{\pi}^{2\pi}\int_{0}^{\infty}\int_{-\infty}^{\infty} \frac{-n_s\beta_{fs}}{MN^6} r\, \mathrm{d}z\, \mathrm{d}r\, \mathrm{d}\theta, \tag{A 3}$$

where V_s is the solid volume, $n_s$is the number density of the solid molecules, and ϕ_{fs} is the van der Waals potential in (3.1). The integrals are evaluated as follows (Wu 2003):

$$\int_{-\infty}^{\infty} \frac{\mathrm{d}z}{[R^2 + r^2 + z^2 - 2rR\cos(\theta - \gamma)]^3} = \frac{3\pi}{8[R^2 + r^2 - 2rR\cos(\theta - \gamma)]^{5/2}}, \tag{A 4}$$

$$\int_{0}^{\infty} \frac{3\pi r\, \mathrm{d}r}{8[R^2 + r^2 - 2rR\cos(\theta - \gamma)]^{5/2}} = \frac{\pi}{8[1 - \cos(\theta - \gamma)]^2 R^3}, \tag{A 5}$$

$$\int \frac{\pi\, \mathrm{d}\theta}{8[1 - \cos(\theta - \gamma)]^2 R^3} = \frac{-\pi}{12R^3 \sin^3(\theta - \gamma)}\left[1 + \tfrac{3}{2}\cos(\theta - \gamma) - \tfrac{1}{2}\cos^3(\theta - \gamma)\right]. \tag{A 6}$$

An integration constant has been omitted in (A 6) since it plays no part in later developments. Thus, (A 3) becomes

$$\Phi_{fs} = -\frac{\pi n_s \beta_{fs}}{6v_1^3}, \tag{A 7}$$

where $v_1 = R\sin\gamma$. Since the solid domain is unbounded in x, Φ_{fs} is independent of x and depends only on v_1, the height of M (figure 2).

The intermolecular potential between point M and the vapour region V_g can be evaluated similarly:

$$\Phi_{fg} = \iiint_{V_g} n_g \phi_{fg}\, \mathrm{d}V = \int_{\psi}^{\pi}\int_{0}^{\infty}\int_{-\infty}^{\infty} \frac{-n_g\beta_{fg}}{MN^6} r\, \mathrm{d}z\, \mathrm{d}r\, \mathrm{d}\theta = \frac{-\pi n_g \beta_{fg}}{6}\left(\frac{a_1 - 1}{v_1^3} + \frac{a_2}{v_2^3}\right), \tag{A 8}$$

where $v_2 = R\sin(\psi - \gamma)$ is the normal distance between M and the wedge surface (figure 2), and

$$a_1 = \tfrac{1}{2} + \tfrac{3}{4}\cos\gamma - \tfrac{1}{4}\cos^3\gamma, \tag{A 9}$$

$$a_2 = \tfrac{1}{2} + \tfrac{3}{4}\cos(\psi - \gamma) - \tfrac{1}{4}\cos^3(\psi - \gamma). \tag{A 10}$$

To calculate Φ_{ff}, it is easier to find the total and the complement, instead of direct integration. The total is the potential between M and an infinite body of liquid V_{-D} outside a sphere of radius D surrounding M:

$$\Phi_{-D} = \iiint_{V_{-D}} n_f \phi_{ff}\mathrm{d}V = \int_{D}^{\infty} -\frac{n_f\beta_{ff}}{r^6}(4\pi r^2)\, \mathrm{d}r = -\frac{4\pi n_f \beta_{ff}}{3D^3}. \tag{A 11}$$

The integration domain V_{-D} is the sum of the liquid domain V_f and the complementary domain $V_s + V_g$. Thus, the total potential is similarly the sum of the liquid potential Φ_{ff} and the complementary potential Φ_C, which is the intermolecular potential between M and the solid and vapour regions when these regions are filled with liquid:

$$\Phi_C = -\frac{\pi n_f \beta_{ff}}{6v_1^3} - \frac{\pi n_f \beta_{ff}}{6}\left(\frac{a_1 - 1}{v_1^3} + \frac{a_2}{v_2^3}\right), \tag{A 12}$$

https://doi.org/10.1017/S0022112004008420 Published online by Cambridge University Press

where the results for Φ_{fs} and Φ_{fg} have been used with $n_s\beta_{fs}$ and $n_g\beta_{fg}$ replaced by $n_f\beta_{ff}$. Thus,

$$\Phi_{ff} = \Phi_{-D} - \Phi_C = -\frac{4\pi n_f\beta_{ff}}{3D^3} + \frac{\pi n_f\beta_{ff}}{6}\left(\frac{a_1}{v_1^3} + \frac{a_2}{v_2^3}\right). \tag{A 13}$$

This solution is symmetric about the bisector of the wedge, as expected.

The total intermolecular potential per unit volume at point M in the liquid is

$$\Phi = n_f(\Phi_{ff} + \Phi_{fs} + \Phi_{fg}) = \frac{\pi n_f^2\beta_{ff}}{6}\left[\frac{a_1(1-\rho)+\rho-\lambda}{v_1^3} + \frac{a_2(1-\rho)}{v_2^3}\right], \tag{A 14}$$

$$\lambda = \frac{n_s\beta_{fs}}{n_f\beta_{ff}}, \tag{A 15}$$

$$\rho = \frac{n_g\beta_{fg}}{n_f\beta_{ff}}, \tag{A 16}$$

where the potential has been increased by a constant value of $4\pi n_f^2\beta_{ff}/3D^3$. The potential Φ holds for wedge angle $\psi < 90°$.

Appendix B. The excess interaction energy E per unit area

From (3.4),

$$E = \int_D^h (\Phi - \Phi_\infty)\,\mathrm{d}y. \tag{B 1}$$

The potential Φ is the total intermolecular potential per unit volume at point M and Φ_∞ is its value far from the substrate (figure 2). The difference depends only on the position of point M. Thus, the integration over y means summing the potential difference as M moves vertically from $y = D$ to h, where D is the cut-off distance in the van der Waals potential. The integration starts at $y = D$ instead of $y = 0$ to avoid unbounded interactions at the liquid–solid interface. The singularity arises because the cut-off sphere surrounding M is assumed to contain only liquid molecules (Appendix A). If M is at the liquid–solid interface, it interacts with adjacent solid molecules, resulting in infinite energy that cannot be prevented by the cut-off liquid sphere. Thus, an additional truncation is needed at the liquid–solid interface. At the liquid–vapour interface, the infinite self-interactions have been eliminated by subtracting Φ_∞ from Φ, and a cut-off is not required.

Substitution of Φ in (3.2) and Φ_∞ in (3.3) into (B 1) yields

$$E = \frac{\pi n_f^2\beta_{ff}}{6}\left[\int_D^h \frac{a_1(1-\rho)+\rho-\lambda}{v_1^3}\,\mathrm{d}y + (1-\rho)\int_D^h \frac{(a_2-1)}{v_2^3}\,\mathrm{d}y\right], \tag{B 2}$$

As the position of M changes, the wedge angle ψ stays fixed, but v_1, v_2, and γ will vary (figure 2). From geometry,

$$v_1 = y, \tag{B 3}$$

$$v_2 = (h-y)\cos\psi, \tag{B 4}$$

$$\cos\psi = \left(1 + h_x^2\right)^{-1/2}, \tag{B 5}$$

$$\cos\gamma = \frac{h}{\left(h^2 + h_x^2y^2\right)^{1/2}}, \tag{B 6}$$

$$\cos(\psi-\gamma) = \left[1 - \frac{h_x^2(h-y)^2}{\left(1+h_x^2\right)\left(h^2+h_x^2y^2\right)}\right]^{1/2}, \tag{B 7}$$

https://doi.org/10.1017/S0022112004008420 Published online by Cambridge University Press

These expressions are substituted into the integrands in (B 2):

$$\int_D^h \frac{a_1(1-\rho)+\rho-\lambda}{v_1^3}\,\mathrm{d}y = \left(\frac{1}{D^2}-\frac{1}{h^2}\right)\left(\frac{1+\rho-2\lambda}{4}\right) + \frac{1-\rho}{4}\left[\frac{h}{D^2\left(h^2+h_x^2D^2\right)^{1/2}}-\frac{1}{h^2\left(1+h_x^2\right)^{1/2}}\right], \quad \text{(B 8)}$$

$$\int_D^h \frac{(a_2-1)}{v_2^3}\,\mathrm{d}y = \frac{\left(1+h_x^2\right)^{3/2}}{4(h-D)^2}-\frac{\left(1+2h_x^2\right)h_x^2}{8h^2\left(1+h_x^2\right)^{1/2}}-\frac{(2h-D)D^2h_x^4+(h+D)h^2h_x^2+h^3}{4(h-D)^2h^2\left[h^2+D^2h_x^2\right]^{1/2}}. \quad \text{(B 9)}$$

The above results are exact. In the limit $D/h \to 0$, the above integrals simplify:

$$E = -\frac{\pi n_f^2\beta_{ff}}{4h^2}\left\{\frac{(1-\lambda)}{3}+\frac{(1-\rho)h_x^2}{4}\left[1-\left(1+h_x^2\right)^{-1/2}\right]\right\}+\frac{\pi n_f^2\beta_{ff}(1-\lambda)}{12D^2}. \quad \text{(B 10)}$$

The last term is constant and can be eliminated since E is a potential.

Appendix C. Asymptotic solution of the valley film profile for $C = 0$

Equation (4.17),

$$H_{\zeta\zeta}-\left(\frac{1-\varepsilon^2H_\zeta^4+2\varepsilon^2HH_\zeta^2H_{\zeta\zeta}}{H^3}\right)=0, \quad \text{(C 1}a\text{)}$$

is subject to the symmetry condition at $\zeta = 0$:

$$H = 1, \quad H_\zeta = 0. \quad \text{(C 1}b,c\text{)}$$

In the limit $\varepsilon \to 0$, the film height can be expanded in an asymptotic series of ε^2:

$$H(\zeta) = H_0(\zeta)+\varepsilon^2H_1(\zeta)+\cdots. \quad \text{(C 2)}$$

Substitution into (C 1) yields

$$H_{0\zeta\zeta}-\frac{1}{H_0^3}+\varepsilon^2\left(H_{1\zeta\zeta}+\frac{3H_1}{H_0^4}-\frac{-H_{0\zeta}^4+2H_0H_{0\zeta}^2H_{0\zeta\zeta}}{H_0^3}\right)=0. \quad \text{(C 3}a\text{)}$$

At $\zeta = 0$,

$$H_0 = 1, \quad H_1 = 0, \quad H_{0\zeta} = H_{1\zeta} = 0. \quad \text{(C 3}b\text{–}d\text{)}$$

An analytic solution is found for H_0:

$$H_0 = (\zeta^2+1)^{1/2}. \quad \text{(C 4)}$$

As $\zeta \to \infty$, $H_{0\zeta} \to 1$. Thus, the leading-order solution captures the asymptotic value of the slope in (4.16).

The first-order expansion H_1 obeys

$$H_{1\zeta\zeta}+\frac{3H_1}{(\zeta^2+1)^2} = -\frac{\zeta^2(\zeta^2-2)}{(\zeta^2+1)^{7/2}}, \quad \text{(C 5)}$$

and at $\zeta = 0$, $H_1 = H_{1\zeta} = 0$. Equation (C 5) admits an analytic solution:

$$H_1 = \frac{\zeta}{4(\zeta^2+1)^{3/2}}[(\zeta^2+1)\tan^{-1}(\zeta)-\zeta]. \quad \text{(C 6)}$$

https://doi.org/10.1017/S0022112004008420 Published online by Cambridge University Press

As $\zeta \to \infty$, $H_1 \to \pi/8 - 1/2\zeta + O(\zeta^{-2})$. The asymptotic solution $H = H_0 + \varepsilon^2 H_1$ is plotted in figure 3 for $\varepsilon = 0.5$.

Appendix D. Drop profile by matched asymptotic expansions

The profile of a drop with positive disjoining pressure obeys (4.6):

$$H_{XX} + \varepsilon \left(\frac{1 - H_X^4 + 2HH_X^2 H_{XX}}{H^3} \right) = C. \tag{D 1}$$

The disjoining pressure demands that near the contact line as $H \to 0$, $H_X \to 1$ and $H_{XX} \to 0$. Setting $\varepsilon = 0$ in (D 1) leaves a second-order differential equation that cannot satisfy all the boundary conditions. Thus, $\varepsilon \to 0$ is singular and an inner region exists near the contact line. In the inner region, the capillary pressure balances the disjoining pressure to yield $\delta H \sim \delta X \sim \varepsilon^{1/2}$, where δH and δX are the length scales of H and X. This suggests that the outer variables should be expanded in series of $\varepsilon^{1/2}$:

$$H = H_0 + \varepsilon^{1/2} H_1 + (\varepsilon \ln \varepsilon) H_2 + \varepsilon H_3 + \cdots, \tag{D 2a}$$

$$C = C_0 + \varepsilon^{1/2} C_1 + (\varepsilon \ln \varepsilon) C_2 + \varepsilon C_3 + \cdots, \tag{D 2b}$$

$$X_0 = X_{00} + \varepsilon^{1/2} X_{01} + (\varepsilon \ln \varepsilon) X_{02} + \varepsilon X_{03} + \cdots, \tag{D 2c}$$

where X_0 is the contact-line position, and the $\varepsilon \ln \varepsilon$ scale is suggested by the inner solution. Substitution into (D 1) leads to

$$H_{0XX} + \varepsilon^{1/2} H_{1XX} + (\varepsilon \ln \varepsilon) H_{2XX} + \varepsilon \left(H_{3XX} + \frac{1 - H_{0X}^4 + 2H_0 H_{0X}^2 H_{0XX}}{H_0^3} \right) = C_0 + \varepsilon^{1/2} C_1 + (\varepsilon \ln \varepsilon) C_2 + \varepsilon C_3. \tag{D 3}$$

At $X = 0$,

$$H_0 + \varepsilon^{1/2} H_1 + (\varepsilon \ln \varepsilon) H_2 + \varepsilon H_3 = 1, \tag{D 4a}$$

$$H_{0X} + \varepsilon^{1/2} H_{1X} + (\varepsilon \ln \varepsilon) H_{2X} + \varepsilon H_{3X} = 0. \tag{D 4b}$$

The leading-order solution is

$$H_0 = \tfrac{1}{2} C_0 X^2 + 1. \tag{D 5}$$

The leading-order pressure jump C_0 can be found by matching.

In the inner region, a set of variables is defined:

$$\eta = \frac{H}{\varepsilon^{1/2}}, \tag{D 6}$$

$$\xi = \frac{X - X_0}{\varepsilon^{1/2}}. \tag{D 7}$$

Equation (D 1) becomes

$$\eta_{\xi\xi} + \frac{1 - \eta_\xi^4 + 2\eta\eta_\xi^2 \eta_{\xi\xi}}{\eta^3} = \varepsilon^{1/2} C. \tag{D 8}$$

At the contact line as $\xi \to 0$, (4.2) requires

$$\eta \to 0, \quad \eta_\xi \to -1, \quad \eta_{\xi\xi} \to 0, \quad \eta_{\xi\xi\xi} \to 0. \tag{D 9}$$

https://doi.org/10.1017/S0022112004008420 Published online by Cambridge University Press

Although (D 8) is only second order, four boundary conditions are needed owing to the singularity at $\eta = 0$.

The inner variable is expanded in series of $\varepsilon^{1/2}$:

$$\eta = \eta_0 + \varepsilon^{1/2}\eta_1 + \varepsilon\eta_2 + \cdots. \tag{D 10}$$

Substitution into (D 8) yields

$$\begin{aligned}
&\eta_{0\xi\xi} + \frac{1-\eta_{0\xi}^4 + 2\eta_0\eta_{0\xi}^2\eta_{0\xi\xi}}{\eta_0^3} + \varepsilon^{1/2}\left[\left(1+\frac{2\eta_{0\xi}^2}{\eta_0^2}\right)\eta_{1\xi\xi} + \left(\eta_{0\xi\xi} - \frac{\eta_{0\xi}^2}{\eta_0}\right)\frac{4\eta_{0\xi}\eta_{1\xi}}{\eta_0^2}\right.\\
&\quad - \left.\left(4\eta_{0\xi}^2\eta_{0\xi\xi} + \frac{3(1-\eta_{0\xi}^4)}{\eta_0}\right)\frac{\eta_1}{\eta_0^3}\right] + \varepsilon\left[\left(1+\frac{2\eta_{0\xi}^2}{\eta_0^2}\right)\eta_{2\xi\xi} + \left(\eta_{0\xi\xi} - \frac{\eta_{0\xi}^2}{\eta_0}\right)\frac{4\eta_{0\xi}\eta_{2\xi}}{\eta_0^2}\right.\\
&\quad - \left(4\eta_{0\xi}^2\eta_{0\xi\xi} + \frac{3(1-\eta_{0\xi}^4)}{\eta_0}\right)\frac{\eta_2}{\eta_0^3} + \left(\eta_{1\xi} - \frac{\eta_{0\xi}\eta_1}{\eta_0}\right)\frac{4\eta_{0\xi}\eta_{1\xi\xi}}{\eta_0^2}\\
&\quad + \left(\eta_{0\xi\xi} - \frac{3\eta_{0\xi}^2}{\eta_0}\right)\frac{2\eta_{1\xi}^2}{\eta_0^2} + \left(\frac{3\eta_{0\xi}^2}{\eta_0} - 2\eta_{0\xi\xi}\right)\frac{4\eta_1\eta_{0\xi}\eta_{1\xi}}{\eta_0^3}\\
&\quad + \left.\frac{6(1-\eta_{0\xi}^4 + \eta_0\eta_{0\xi}^2\eta_{0\xi\xi})\eta_1^2}{\eta_0^5}\right] = \varepsilon^{1/2}C_0 + \varepsilon C_1.
\end{aligned} \tag{D 11}$$

To leading order,

$$\eta_{0\xi\xi} + \frac{1-\eta_{0\xi}^4 + 2\eta_0\eta_{0\xi}^2\eta_{0\xi\xi}}{\eta_0^3} = 0. \tag{D 12}$$

This equation is the same as (4.6) with $C = 0$ and $\varepsilon = 1$. From § 4.1, the only solution that contacts the substrate is

$$\eta_0 = -\xi. \tag{D 13}$$

This is to be matched to the outer solution.

Inner and outer expansions are matched by taking the outer limit of the inner expansions and the inner limit of the outer expansions:

$$\lim_{X\to X_0} H = \lim_{\xi\to-\infty} \varepsilon^{1/2}\eta. \tag{D 14}$$

In the limit $X \to X_0 = X_{00}$,

$$H_0 \to \tfrac{1}{2}C_0(X - X_0)^2 + C_0X_{00}(X - X_0) + \tfrac{1}{2}C_0X_{00}^2 + 1. \tag{D 15}$$

In the limit $\xi \to -\infty$,

$$\varepsilon^{1/2}\eta_0 \to -(X - X_0). \tag{D 16}$$

Matching (D 15) and (D 16) yields

$$X_{00} = 2, \tag{D 17}$$

$$C_0 = -\tfrac{1}{2}. \tag{D 18}$$

This completes the zero-order expansions.

The first-order outer solution is

$$H_1 = \tfrac{1}{2}C_1X^2, \tag{D 19}$$

https://doi.org/10.1017/S0022112004008420 Published online by Cambridge University Press

where C_1 has to be found by matching. The first-order inner film height obeys

$$\eta_{1\xi\xi} - \frac{4}{\xi(\xi^2+2)}\eta_{1\xi} = \frac{-\xi^2}{2(\xi^2+2)}. \tag{D 20}$$

As $\xi \to 0$, (D 9) shows that

$$\eta_1, \eta_{1\xi}, \eta_{1\xi\xi}, \eta_{1\xi\xi\xi} \to 0. \tag{D 21}$$

An analytical solution is found:

$$\eta_1 = -\tfrac{1}{4}\xi^2 + \tfrac{1}{2}\ln\left(\frac{\xi^2+2}{2}\right). \tag{D 22}$$

The matching principle (D 14) is invoked again. In the limit $X \to X_0 = X_{00} + \varepsilon^{1/2}X_{01}$,

$$\begin{aligned} H_0 + \varepsilon^{1/2}H_1 \to {} & -\tfrac{1}{4}(X-X_0)^2 - (X-X_0) \\ & + \varepsilon^{1/2}\left[\tfrac{1}{2}C_1(X-X_0)^2 + \left(2C_1 - \tfrac{1}{2}X_{01}\right)(X-X_0) + 2C_1 - X_{01}\right]. \end{aligned} \tag{D 23}$$

In the limit $\xi \to -\infty$,

$$\varepsilon^{1/2}\eta_0 + \varepsilon\eta_1 \to -\tfrac{1}{4}(X-X_0)^2 - (X-X_0). \tag{D 24}$$

Matching (D 23) and (D 24) yields

$$X_{01} = C_1 = 0. \tag{D 25}$$

This completes the first-order expansions.

At the $\varepsilon \ln \varepsilon$ order, the outer expansion obeys

$$H_{2XX} = C_2. \tag{D 26}$$

Its solution that satisfies the boundary conditions in (D 4) is

$$H_2 = \tfrac{1}{2}C_2X^2. \tag{D 27}$$

This needs to be matched together with the order-ε outer expansion, which solves

$$H_{3XX} = C_3 - \frac{16}{(X^2-4)^2}. \tag{D 28}$$

By imposing the conditions $H_3 = H_{3X} = 0$ at $X = 0$, we find

$$H_3 = \frac{1}{2}C_3X^2 + \frac{X}{2}\ln\left(\frac{2-X}{2+X}\right). \tag{D 29}$$

The inner second-order expansion obeys

$$\eta_{2\xi\xi} - \frac{4}{\xi(\xi^2+2)}\eta_{2\xi} = \frac{\xi^3[\xi^4 + 10\xi^2 - 4(\xi^2+2)\ln(\xi^2/2+1)]}{2(\xi^2+2)^4}. \tag{D 30}$$

As $\xi \to 0$, (D 9) shows that

$$\eta_2, \eta_{2\xi}, \eta_{2\xi\xi}, \eta_{2\xi\xi\xi} \to 0. \tag{D 31}$$

An analytical solution is found:

$$\eta_2 = \frac{\xi^3\ln(1+\xi^2/2)}{4(\xi^2+2)} - \frac{\xi(6\xi^4+25\xi^2+30)}{8(\xi^2+2)^2} + \frac{15\sqrt{2}}{16}\tan^{-1}\left(\frac{\xi}{\sqrt{2}}\right). \tag{D 32}$$

https://doi.org/10.1017/S0022112004008420 Published online by Cambridge University Press

In the limit $X \to X_0 = X_{00} + (\varepsilon \ln \varepsilon) X_{02} + \varepsilon X_{03}$,

$$\begin{aligned} H_0 + \varepsilon^{1/2} H_1 + (\varepsilon \ln \varepsilon) H_2 + \varepsilon H_3 \to & -\tfrac{1}{4}(X - X_0)^2 - (X - X_0) \\ & + (\varepsilon \ln \varepsilon)\left[\tfrac{1}{2} C_2 (X - X_0)^2 + (X - X_0)\left(2C_2 - \tfrac{1}{2} X_{02}\right) + 2C_2 - X_{02}\right] \\ & + \varepsilon \left[\ln(X_0 - X) + \tfrac{1}{2}(X - X_0)\ln(X_0 - X) + (X - X_0)^2\left(\tfrac{1}{2} C_3 - \tfrac{3}{32}\right)\right. \\ & \left. + (X - X_0)\left(2C_3 - \tfrac{1}{2} X_{03} - \tfrac{1}{4} - \ln 2\right) + 2C_3 - X_{03} - 2\ln 2\right]. \end{aligned} \tag{D 33}$$

In the limit $\xi \to -\infty$,

$$\begin{aligned} \varepsilon^{1/2}\eta_0 + \varepsilon\eta_1 + \varepsilon^{3/2}\eta_2 \to & -\tfrac{1}{4}(X - X_0)^2 - (X - X_0) + (\varepsilon \ln \varepsilon)\left[-\tfrac{1}{4}(X - X_0) - \tfrac{1}{2}\right] \\ & + \varepsilon \left[\ln(X_0 - X) + \tfrac{1}{2}(X - X_0)\ln(X_0 - X) - \tfrac{1}{4}(3 + \ln 2)(X - X_0) - \tfrac{1}{2}\ln 2\right]. \end{aligned} \tag{D 34}$$

Matching (D 33) and (D 34) yields

$$C_2 = 0, \tag{D 35}$$

$$X_{02} = \tfrac{1}{2}, \tag{D 36}$$

$$C_3 = -\tfrac{1}{2}, \tag{D 37}$$

$$X_{03} = -1 - \tfrac{3}{2}\ln 2. \tag{D 38}$$

This completes the third-order expansions.

Appendix E. An asymptotic solution of the wedge film

The wedge film that starts at the contact line and grows to a constant-curvature surface (C = 1) obeys (4.37). Near the contact line at $X = 0$, $H \to 0$, $H_X \to 1$, $H_{XX} \to 0$, and $H_{XXX} \to 0$. The last two conditions cannot be satisfied if $\varepsilon = 0$. Thus, an inner region exists near the contact line in which the capillary pressure balances the disjoining pressure to yield the length scales of H and X as $\delta H \sim \delta X \sim \varepsilon^{1/2}$. Hence, the film height is expanded in a series of $\varepsilon^{1/2}$ as in (4.39). Substitution of the series into (4.37) leads to

$$H_{0XX} + \varepsilon^{1/2} H_{1XX} + (\varepsilon \ln \varepsilon) H_{2XX} + \varepsilon \left(H_{3XX} + \frac{1 - H_{0X}^4 + 2H_0 H_{0X}^2 H_{0XX}}{H_0^3} \right) = 1. \tag{E 1}$$

The leading-order solution is

$$H_0 = \tfrac{1}{2} X^2 + k_1 X + k_2. \tag{E 2}$$

The integration constants can be found by matching.

The film height in the inner region obeys

$$\eta_{\xi\xi} + \frac{1 - \eta_\xi^4 + 2\eta\eta_\xi^2\eta_{\xi\xi}}{\eta^3} = \varepsilon^{1/2}, \tag{E 3}$$

obtained by substituting the inner variables in (4.40) into (4.37). At the contact line as $\xi \to 0$, (4.2) requires

$$\eta \to 0, \quad \eta_\xi \to 1, \quad \eta_{\xi\xi} \to 0, \quad \eta_{\xi\xi\xi} \to 0. \tag{E 4}$$

The inner expansion in (4.41) is substituted into (E 3) to yield an equation the same as (D 11) except that the right-hand side is $\varepsilon^{1/2}$. The leading-order expansion obeys

https://doi.org/10.1017/S0022112004008420 Published online by Cambridge University Press

(D 12) and its solution subject to (E 4) is

$$\eta_0 = \xi. \tag{E 5}$$

This is to be matched to the outer solution.

Inner and outer expansions are matched by taking the appropriate limits:

$$\lim_{X\to 0} H = \lim_{\xi\to\infty} \varepsilon^{1/2}\eta. \tag{E 6}$$

In the limit $X \to 0$,

$$H_0 \to \tfrac{1}{2}X^2 + k_1 X + k_2. \tag{E 7}$$

In the limit $\xi \to \infty$,

$$\varepsilon^{1/2}\eta_0 \to X. \tag{E 8}$$

Matching (E 7) and (E 8) yields

$$k_1 = 1, \tag{E 9}$$

$$k_2 = 0. \tag{E 10}$$

This completes the zero-order expansions.

The first-order outer solution is

$$H_1 = k_3 X + k_4. \tag{E 11}$$

The first-order inner film height obeys

$$\eta_{1\xi\xi} - \frac{4}{\xi(\xi^2+2)}\eta_{1\xi} = \frac{\xi^2}{\xi^2+2}. \tag{E 12}$$

As $\xi \to 0$, (E 4) shows that

$$\eta_1, \eta_{1\xi}, \eta_{1\xi\xi}, \eta_{1\xi\xi\xi} \to 0. \tag{E 13}$$

An analytical solution is found:

$$\eta_1 = \tfrac{1}{2}\xi^2 - \ln\left(\frac{\xi^2+2}{2}\right). \tag{E 14}$$

The matching principle (E 6) is invoked again. In the limit $X \to 0$,

$$H_0 + \varepsilon^{1/2}H_1 \to \tfrac{1}{2}X^2 + X + \varepsilon^{1/2}(k_3 X + k_4). \tag{E 15}$$

In the limit $\xi \to \infty$,

$$\varepsilon^{1/2}\eta_0 + \varepsilon\eta_1 \to \tfrac{1}{2}X^2 + X + \varepsilon\ln\varepsilon - \varepsilon(2\ln X - \ln 2). \tag{E 16}$$

Matching (E 15) and (E 16) yields

$$k_3 = k_4 = 0. \tag{E 17}$$

This completes the first-order expansions.

At the $\varepsilon\ln\varepsilon$ order, the outer expansion obeys

$$H_{2XX} = 0. \tag{E 18}$$

Its solution is

$$H_2 = k_5 X + k_6. \tag{E 19}$$

https://doi.org/10.1017/S0022112004008420 Published online by Cambridge University Press

This needs to be matched together with the order-ε outer expansion, which solves

$$H_{3XX} = \frac{8}{X^2(X+2)^2}. \tag{E 20}$$

We find

$$H_3 = 2(X+1)\ln\left(\frac{X+2}{X}\right) + k_7 X + k_8. \tag{E 21}$$

The inner second-order expansion obeys

$$\eta_{2\xi\xi} - \frac{4}{\xi(\xi^2+2)}\eta_{2\xi} = -\frac{2\xi^3[\xi^4+10\xi^2-4(\xi^2+2)\ln(\xi^2/2+1)]}{(\xi^2+2)^4}. \tag{E 22}$$

This equation with the boundary conditions derived from (E4) that, as $\xi \to 0$,

$$\eta_2, \eta_{2\xi}, \eta_{2\xi\xi}, \eta_{2\xi\xi\xi} \to 0, \tag{E 23}$$

has an analytical solution:

$$\eta_2 = \frac{\xi(6\xi^4+25\xi^2+30)}{2(\xi^2+2)^2} - \frac{\xi^3\ln(\xi^2/2+1)}{\xi^2+2} - \frac{15\sqrt{2}}{4}\tan^{-1}\left(\frac{\xi}{\sqrt{2}}\right). \tag{E 24}$$

In the limit $X \to 0$,

$$H_0 + \varepsilon^{1/2}H_1 + (\varepsilon\ln\varepsilon)H_2 + \varepsilon H_3 \to \tfrac{1}{2}X^2 + X + (\varepsilon\ln\varepsilon)(k_5 X + k_6) + \varepsilon[2(X+1)(\ln 2 - \ln X) + k_7 X + k_8]. \tag{E 25}$$

In the limit $\xi \to \infty$,

$$\varepsilon^{1/2}\eta_0 + \varepsilon\eta_1 + \varepsilon^{3/2}\eta_2 \to \tfrac{1}{2}X^2 + X + (\varepsilon\ln\varepsilon)(X+1) + \varepsilon[(3+\ln 2)X - 2(X+1)\ln X + \ln 2]. \tag{E 26}$$

Matching (E 25) and (E 26) yields

$$k_5 = 1, \tag{E 27}$$

$$k_6 = 1, \tag{E 28}$$

$$k_7 = 3 - \ln 2, \tag{E 29}$$

$$k_8 = -\ln 2. \tag{E 30}$$

This completes the third-order expansions.

REFERENCES

Barrat, J. & Bocquet, L. 1999 Large slip effect at a nonwetting fluid-solid interface. *Phys. Rev. Lett.* **82**, 4671–4674.

Courant, R. & Hilbert, D. 1953 *Methods of Mathematical Physics*. Interscience.

Davis, J. M. & Troian, S. M. 2003 Influence of attractive van der Waals interactions on the optimal excitations in thermocapillary-driven spreading. *Phys. Rev.* E **67**, 016308.

Derjaguin, B., Zorin, Z. M., Churaev, N. V. & Shishin, V. A. 1978 Examination of thin layers on various solid substrates. In *Wetting, Spreading and Adhesion* (ed. J. F. Padday). Academic.

Deryagin, B. V., Starov, V. M. & Churaev, N. V. 1976 Profile of the transition zone between a wetting film and the meniscus of the bulk liquid. *Colloid J.* **38**, 875–879.

https://doi.org/10.1017/S0022112004008420 Published online by Cambridge University Press

Dussan V., E. B. 1979 On the spreading of liquids on solid surfaces: static and dynamic contact lines. *Annu. Rev. Fluid. Mech.* **11**, 371–400.

Dussan V., E. B. & Davis, S. H. 1974 On the motion of a fluid-fluid interface along a solid surface. *J. Fluid Mech.* **65**, 71–95.

Hocking, L. M. 1993 The influence of intermolecular forces on thin fluid layers. *Phys. Fluids* **5**, 793–799.

Indeikina, A. & Chang, H. C. 1999 A molecular theory for dynamic contact angles. In *IUTAM Symp. on Non-Linear Singularities in Deformation and Flow* (ed. D. Durban & J. R. A. Pearson). Kluwer.

Israelachvili, J. 1992 *Intermolecular and Surface Forces.* Academic.

Ivanov, I. B. 1988 *Thin Liquid Films: Fundamentals and Applications.* Marcel Dekker.

Jensen, O. E. & Grotberg, J. B. 1992 Insoluble surfactant spreading on a thin viscous film: shock evolution and film rupture. *J. Fluid Mech.* **240**, 259–288.

Koplik, J., Banavar, J. R. & Willemsen, J. F. 1989 Molecular dynamics of fluid flow at solid surfaces. *Phys. Fluids* A **1**, 781–794.

Kovscek, A. R., Wong, H. & Radke, C. J. 1993 A pore-level scenario for the development of mixed wettability in oil reservoirs. *AIChE J.* **39**, 1072–1085.

Lee, S. & Sigmund, W. M. 2002 AFM study of repulsive van der Waals forces between Teflon AF thin film and silica or alumina. *Colloids Surf.* A **204**, 43–50.

Levich, V. G. 1962 *Physicochemical Hydrodynamics.* Prentice-Hall.

Mahanty, J. & Ninham, B. W. 1976 *Dispersion Forces.* Academic.

Merchant, G. J. & Keller, J. B. 1992 Contact angles. *Phys. Fluids* A **4**, 477–485.

Miller, C. A. & Ruckenstein, E. 1974 The origin of flow during wetting of solids. *J. Colloid Interface Sci.* **48**, 368–373.

Oron, A., Davis, S. H. & Bankoff, S. G. 1997 Long-scale evolution of thin liquid films. *Rev. Mod. Phys.* **69**, 931–980.

Pismen, L. M., Rubinstein, B. Y. & Bazhlekov, I. 2000 Spreading of a wetting film under the action of van der Waals forces. *Phys. Fluids* **12**, 480–483.

Reiter, G., Sharma, A., Casoli, A., David, M., Khanna, R. & Auroy, P. 1999 Thin film instability induced by long-range forces. *Langmuir* **15**, 2551–2558.

Renk, F., Wayner, P. C. & Homsy, G. M. 1978 On the transition between a wetting film and a capillary meniscus. *J. Colloid Interface Sci.* **67**, 408–414.

Ruckenstein, E. & Jain, R. K. 1974 Spontaneous rupture of thin liquid films. *J. Chem. Soc. Faraday Trans.* II **70**, 132–147.

Shikhmurzaev, Y. D. 1997 Moving contact lines in liquid/liquid/solid systems. *J. Fluid Mech.* **334**, 211–249.

Thompson, P. A. & Robbins, M. O. 1989 Simulations of contact-line motion: slip and the dynamic contact angle. *Phys. Rev. Lett.* **63**, 766–769.

Vaynblat, D., Lister, J. R. & Witelski, T. P. 2001 Rupture of thin viscous films by van der Waals forces: evolution and self-similarity. *Phys. Fluids* **13**, 1130–1140.

Wong, H., Fatt, I. & Radke, C. J. 1996 Deposition and thinning of the human tear film. *J. Colloid Interface Sci.* **184**, 44–51.

Wong, H., Morris, S. & Radke, C. J. 1992*a* Two-dimensional menisci in non-axisymmetric capillaries. *J. Colloid Interface Sci.* **148**, 284–287.

Wong, H., Morris, S. & Radke, C. J. 1992*b* Three-dimensional menisci in polygonal capillaries. *J. Colloid Interface Sci.* **148**, 317–336.

Wong, H., Rumschitzki, D. & Maldarelli, C. 1999 Marangoni effects on the motion of an expanding or contracting bubble pinned at a submerged tube tip. *J. Fluid Mech.* **379**, 279–302.

Wu, Q. 2003 A disjoining pressure for small contact angles and its applications. Master thesis, Louisiana State University.

Yeh, E. K., Newman, J. & Radke, C. J. 1999 Equilibrium configurations of liquid droplets on solid surfaces under the influence of thin-film forces. Part I. Thermodynamics. *Colloids Surf.* A **156**, 137–144.

Zhang, W. W. & Lister, J. R. 1999 Similarity solutions for van der Waals rupture of a thin film on a solid substrate. *Phys. Fluids* **11**, 2454–2462.

https://doi.org/10.1017/S0022112004008420 Published online by Cambridge University Press